MOLECULAR DYNAMICS MODELING OF NORMAL SHOCK WAVES IN MONATOMIC AND POLYATOMIC GAS MIXTURES

A THESIS
SUBMITTED TO THE FACULTY OF THE GRADUATE SCHOOL
OF THE UNIVERSITY OF MINNESOTA
BY

PATRICK ALAN TUMP

IN PARTIAL FULFILLMENT OF THE REQUIREMENTS
FOR THE DEGREE OF
MASTER OF SCIENCE

THOMAS E. SCHWARTZENTRUBER

SEPTEMBER 2011

Acknowledgements

I would like to acknowledge Paolo Valentini and Professor Schwartzentruber for their outstanding ability to teach the intricacies of MD and for providing many hours of help in this research.

The research is supported by Air Force Office of Scientific Research (AFOSR) under Grant No. FA9550-10-1-0075. The views and conclusions contained herein are those of the author and should not be interpreted as necessarily representing the official policies or endorsements, either expressed or implied, of the AFOSR or the U.S. Government.

Dedication

This thesis is dedicated in loving memory to my father

Ronald Scott Tump

Abstract

Large-scale molecular dynamics (MD) simulations using the Lennard-Jones potential are performed to study the structure of normal shock waves in dilute Nitrogen and mixtures of Helium-Argon and Helium-Xenon. The use of realistic MD simulations of normal shock waves promises to provide a more detailed solution than can be provided experimentally, providing a means to validate and create better DSMC models. MD simulations of Nitrogen and Helium-Argon mixtures show promising comparisons to experimental results, with near perfect agreement between MD and DSMC using Generalized Hard Sphere (GHS).

Table of Contents

List of Figures

1 Introduction

The structure of a normal shock wave can be characterized as a strong, irreversible, one-dimensional, non-equilibrium flow field. These characteristics provide insight into non-equilibrium collision, thermal, and chemical processes of real gases. Modeling of these characteristics is critical to application including atmospheric re-entry or free-expansion jets used in semiconductor fabrication. Therefore, the normal shock wave provides the means to compare and validate a modeling process under highly non-equilibrium conditions.

The need to provide an experimental comparison to analytical and numerical solutions prompted a large number of experimental studies. Some of these include Harnett and Muntz[1], Robben and Talbot[2], and Alsmeyer[3]. In these cases, density profiles and velocity distributions were measured using a fluorescence electron beam technique which requires electrons to travel through a chamber at fairly low pressure and density, i.e., $\sim 10^{-4}$ kg/m^3.

Numerical solution, including those from Bird[4], Hassan and Hash[5], and Matsumoto[6], using variations of the Direct Simulation Monte Carlo (DSMC) method are able to very efficiently obtain solutions to non-equilibrium flows, where a normal shock wave can easily be simulated on a standard computer. In order to model real gas effects such as translational, rotational and vibrational non-equilibrium, DSMC uses several sophisticated collision models, including generalized hard sphere and Variable Hard Sphere (VHS) models. Most DSMC models have been designed to reproduce the empirical laws based on near-equilibrium conditions, with the assumption that they will

also describe extreme non-equilibrium. Unfortunately, current experimental data provides limited data to construct or validate such DSMC collision models.

Molecular Dynamics (MD) provides a means to directly simulate atomic systems through increasingly realistic and transferable empirical interatomic potentials, such as the Lennard-Jones potential (LJ). This allows the description of both equilibrium and non-equilibrium states with only the *a priori* knowledge of the potential energy functions, which remain constant. Unfortunately, relative to DSMC, MD is extremely computationally expensive, making it impractical for large-scale simulations. Therefore, it would be desirable to use MD to simulate a normal shock wave using transferable and accurate potentials to provide a complete solution with the least physical approximations, enabling the construction and validation of DSMC collision models to a finer detail than is available experimentally. In turn, DSMC can then be applied to larger scale applications.

Of course, MD also requires experimental validation. While it would be desirable to directly simulate the conditions typical of experiment, i.e., rarefied conditions, it is computationally prohibitive. Kinetic theory shows that the mean collision time, τ, scales as $\sim 1/\rho\sqrt{T}$. This leads to a mean collision time for a very dilute gas ($\rho \sim 10^{-3}$ kg/m^3) of the order of 10^{-6} seconds. However, because MD integrates the trajectory for every atom, a time step of the order of 10^{-15} seconds is needed to accurately resolve atomic interactions. For this reason, MD simulations with densities on the order of $\rho \sim 1$ kg/m^3 are used and non-dimensionalized to compare to experimental data. Rarefied gas regimes are, however, exactly where DSMC is most efficient. For this reason, after

experimentally validating computationally expensive MD simulations, they are to be used to inform and validate DSMC collision models; and the normal shock waves constitute the ideal validation problem due to its ability to be fully simulated using MD and its highly non-equilibrium nature.

Summarizing the objectives of this thesis, MD is to be used to simulate normal shock waves in Nitrogen and mixtures of Helium-Argon and Helium-Xenon using the realistic Lennard-Jones potential. These include free stream conditions of 11.5% Argon-88.5% Helium, 24.7% Argon-75.3% Helium, 44% Argon-56% Helium, 50% Argon-50% Helium, 1.5% Xenon-98.5% Helium, and Nitrogen at Mach numbers of 1.58, 1.63, 1.65, 10, 3.61, and 7, respectively. Comparisons between MD and experimental data are made for 11.5%-Argon, 24.7%-Argon, 44%-Argon, and Nitrogen. Comparisons between MD and DSMC simulations are made for 11.5%-Argon, 1.5%-Xenon, and 50%-Argon. This is a continuation of work done by Valentini and Schwartzentruber[7], in which the comparison between MD and DSMC for normal shock waves of pure Argon were considered.

This thesis is organized as follows: Section 2 contains a description of the MD technique employed, including a detailed description of boundary conditions, particle generation, and sampling routines; Section 3 contains results and discussions for gas mixtures and Nitrogen for both experimental and DSMC comparisons; Section 4 contains the summary and conclusions.

2 Numerical Method

2.1 Numerical Parameters of Molecular Dynamics (MD)

The classical MD technique integrates the trajectory of particles interacting through a prescribed potential. The word *classical* signifies that quantum effects are neglected and atoms are modeled as material points obeying the laws of Newtonian mechanics. The MD solver used is the Large-Scale Atomic/Molecular Massively Parallel Simulator, LAMMPS. Particle interactions are modeled by the Lennard-Jones potential energy function:[8]

$$\psi(r_{ij}) = 4\epsilon\left[\left(\frac{\sigma}{r_{ij}}\right)^{12} - \left(\frac{\sigma}{r_{ij}}\right)^{6}\right] \quad r_{ij} < r_{in} \tag{2.1}$$

$$r_{ij} = \|\boldsymbol{r}_i - \boldsymbol{r}_j\| \tag{2.2}$$

to a distance $r_{in} = 8$ Å where *i* and *j* denote two interacting particles with position vector $\boldsymbol{r}$ separated by a distance of r_{ij}. The depth of the potential well ϵ and the finite distance at which the inter-particle potential is zero σ are well defined experimentally for interactions where *i* and *j* are like particles. Values for ϵ and σ used in this thesis for Helium-Helium[15] are 0.0203 Kcal/mol and 2.576 Å, Argon-Argon[15] are 0.246 Kcal/mol and 3.418 Å, Xenon-Xenon[19] are 0.455 Kcal/mol and 4.06 Å, and atomic Nitrogen-Nitrogen[21] are 0.0938 Kcal/mol and 3.17 Å, respectively.

For interactions between unlike particles, the parameters ϵ_{ij} and σ_{ij} are approximated by:[8]

$$\epsilon_{ij} = \sqrt{\epsilon_i \epsilon_j} \tag{2.3}$$

$$\sigma_{ij} = \frac{\sigma_i + \sigma_j}{2} \tag{2.4}$$

in which *i* and *j* signify the inter-atomic potential between like particles. For atoms *i* of mass m_i their equations of motion:

$$\dot{\boldsymbol{r}}_i = \boldsymbol{v}_i \tag{2.5}$$

$$\boldsymbol{F}_i(r_{ij}) = m_i \dot{\boldsymbol{v}}_i = \sum_{j=1}^{N} \frac{d\psi(r_{ij})}{dr_{ij}} \frac{\boldsymbol{r}_{ij}}{r_{ij}} \tag{2.6}$$

are integrated in time using the second-order accurate velocity Verlet scheme[8] consistent with a microcanonical ensemble with a time step of 1 fs where $\boldsymbol{v}_i = (v_x, v_y, v_z)$ is the molecular velocity vector. *N* denotes the number of particles interacting with particle *i*, which are within a cutoff distance $r_c = 10$ Å.

A force smoothing is applied between r_{in} and r_c to avoid discontinuities in energy and forces:[8]

$$\boldsymbol{F}_i(r_{ij}) = C_1 + C_2(r_{ij} - r_{in}) + C_3(r_{ij} - r_{in})^2 + C_4(r_{ij} - r_{in})^3 \quad r_{in} < r_{ij} < r_c \qquad (2.7)$$

The polynomial coefficients C_1, C_2, C_3, and C_4 are computed by LAMMPS to cause the force to vary smoothly from r_{in} to r_c where the force and its first derivative will be zero at r_c. Each particle contains a pairwise neighbor list of possible force interactions. All atom pairs within a neighbor cutoff distance equal to r_c plus a *skin* distance of 2.5 Å are stored in the list. This list is updated every 10 time steps using a binning algorithm that scales linearly with N/P where N equals the total number of atoms and P equals the number of processors being used. Values stated for the time step, r_{in}, r_c, and refresh rate of the neighbor lists are default values assigned by LAMMPS. The default *skin* distance of 2 Å was increased to 2.5 Å with no appreciable differences in the results.

For diatomic molecules in which atoms *i* and *j* are bonded, interactions are modeled by the harmonic potential energy function:[8]

$$E(r_{ij}) = \frac{1}{2}K(r_{ij} - r_0)^2 \qquad (2.8)$$

where K is a force constant and r_0 is the equilibrium bond distance. The force constant and equilibrium bond distance for diatomic Nitrogen are 2295 N/m and 1.098 Å, respectively.[15] However, in the simulations considered here, Nitrogen is modeled as a

rigid rotor. Therefore, after each time step, the bond between atoms *i* and *j* is reset to r_0 using the *shake* algorithm in which an additional constraint force is applied so that the new positions of atoms *i* and *j* preserve the equilibrium bond distance. The treatment of diatomic molecules as rigid rotors is followed in order to simulate low temperature conditions investigated in this thesis where vibrational energy excitation is minimal.

2.2 Boundary Conditions and Processes

The one-dimensional nature of a normal-shock wave only imposes a discontinuity along the flow direction, which is the *x*-axis in the simulations presented in this thesis. For this reason a periodic boundary condition can be used in the *y* and *z* direction, but not in the *x* direction; however, for simplicity within LAMMPS, all boundary conditions including the *x*-direction are periodic in nature. To enforce the non-periodic nature along the *x*-axis, the flow domain $\mathcal{D}$ can be decomposed into four regions, $\mathcal{D}_U$, $\mathcal{D}_{MD}$, $\mathcal{D}_D$, and $\mathcal{D}_V$, as shown in Figure 2.1. The region $\mathcal{D}_{MD}$ contains the shock while regions $\mathcal{D}_U$ and $\mathcal{D}_D$ contain a reservoir of particles at the free stream supersonic inflow and subsonic outflow boundary conditions respectively. Region $\mathcal{D}_V$ contains a vacuum to prevent mixing of particles between regions $\mathcal{D}_U$ and $\mathcal{D}_D$.

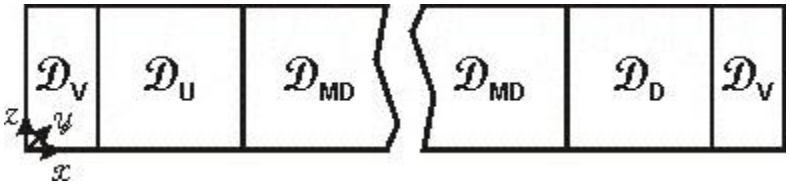

Figure 2.1: MD Box Sub-Domains.

The subsonic inflow and subsonic outflow free stream conditions are known *a priori* by the inflow temperature T_1, density ρ_1, and Mach number M_1. The outflow temperature T_2, density ρ_2, and Mach number M_2 are approximated by the Rankine-Hugoniot conditions:[9]

$$M_2 = \sqrt{\frac{1 + \frac{\gamma - 1}{2} {M_1}^2}{\gamma {M_1}^2 - \frac{\gamma - 1}{2}}} \tag{2.9}$$

$$T_2 = T_1 \left(1 + \frac{2\gamma}{\gamma + 1}\left({M_1}^2 - 1\right)\right)\left(\frac{2 + (\gamma - 1){M_1}^2}{(\gamma + 1){M_1}^2}\right) \tag{2.10}$$

$$\rho_2 = \rho_1 \left(\frac{(\gamma + 1){M_1}^2}{2 + (\gamma - 1){M_1}^2}\right) \tag{2.11}$$

In the simulations considered in this thesis, the inflow Mach number M_1 and temperature T_1 are typically predefined; while the density ρ_1 is chosen to be as large as possible (resulting in the smallest-collision-time) ensuring the gas can still be described as dilute.

At time $t = 0$, atoms are generated within $\mathcal{D}_U$, $\mathcal{D}_{MD}$, and $\mathcal{D}_D$ according to the inflow and outflow conditions with a discontinuity between the two conditions at the center of $\mathcal{D}_{MD}$ along the *x*-axis to initiate the shock. Because the Lennard-Jones potential energy goes to $+\infty$ as the $\lim_{r_{ij} \to 0^+} \psi(r_{ij})$, a conjugate gradient routine minimizes the potential energy of all atoms within $\mathcal{D}$ by iteratively adjusting atom coordinates. This

prevents any non-physical overlaps which may have occurred during the generation of the atoms. During the energy minimization a soft potential energy function is used to model pairwise interactions:[8]

$$E_{soft}(r_{ij}) = \epsilon\left[1 + \cos\left(\frac{\pi r_{ij}}{r_c}\right)\right] \quad r_{ij} < r_c \tag{2.12}$$

The advantages of using a soft potential energy function are twofold. First, $E_{soft}(0) = 2\epsilon$, which prevents an infinite force from being applied to overlapping atoms during minimization. Second, there is no attractive force as is found in the Lennard-Jones potential. This insures all overlapping atoms will be repositioned to a distance $r_{ij} = r_c$ from each other. The attractive force associated with the Lennard-Jones potential forces atoms to unrealistically clump together during an energy minimization.
Once the energy minimization is complete, the MD system is evolved in time Δt, at which point particles within $\mathcal{D}_U$, $\mathcal{D}_D$, and $\mathcal{D}_V$ are removed and then regenerated within $\mathcal{D}_U$ and $\mathcal{D}_D$. An energy minimization is once again performed on newly generated atoms to prevent overlap. The MD system is then evolved in time an additional Δt at which point the process is repeated indefinitely.

The time the system is allowed to evolve Δt is much less than the mean collision time τ between particles, typically several thousand time steps. This allows atoms to travel between sub-domains $\mathcal{D}_U$, $\mathcal{D}_{MD}$, and $\mathcal{D}_D$, enforcing the non-periodic nature along the flow field of the shock within $\mathcal{D}_{MD}$ while ensuring no interaction between sub-domains $\mathcal{D}_{MD}$ and the periodic vacuum $\mathcal{D}_V$. The lengths of sub-domains $\mathcal{D}_U$, $\mathcal{D}_D$, and $\mathcal{D}_V$

are set to ensure the drift of particles through each domain is no more than 1/3 their total length; however, this typically is set much higher. The length of $\mathcal{D}_{MD}$ is set to encompass the length of the shock while providing a smooth transition between inflow and out flow conditions, typically at least 30 free stream mean free paths, λ_1. The dimensions of $\mathcal{D}$ in the *y* and *z* direction are at least $2.5r_C$ to prevent atoms from interacting with their own image due to the periodic boundaries in those directions. However, these are often much larger and adjusted to maintain an overall volume containing a reasonable number of simulated atoms, typically between 1×10^5 and 2×10^5 atoms.

It should be noted that the length of domain $\mathcal{D}$ for all gas mixtures presented in this thesis containing a gas mixture were confined to a maximum length of 9×10^4Å. This was due to a resolved error in which lengths of over 10^5Å would reduce the accuracy of the atoms' spatial positions to 1Å. This would occasionally cause an unrealistic overlap between neighboring particles, forcing them to accelerate to unrealistic speeds. The density ρ_1 was therefore chosen to produce a shock that would fit within this confined length. As a result, the inflow and outflow number density notably did not approximate that of a non-interacting gas. The generation of atoms assumes no potential energy between particles exists. As the number density of the system increases, a larger percentage of the total energy is stored in potential energy, effectively decreasing the overall temperature of the system and in turn affecting density and velocity. This effect is most noticeable in the sub-domain $\mathcal{D}_D$ of low temperature systems due to the higher number density of the outflow and constant removal and regeneration of particles. However, the effect on the overall solution is minimal, for example the inflow and

outflow temperatures are found to drift less than 2% from set conditions. The effects of potential energy exist in all simulations; however, if the precision in LAMMPS input/output files are increased then the length $\mathcal{D}$ can be increased and a lower density may be used. Other techniques to minimize this effect include using a higher inflow temperature to increase the ratio of kinetic energy to potential energy and allowing the system to evolve for a longer Δt, decreasing the number of times particles must be removed and regenerated.

2.3 Generation of Atomistic System

The number of atoms of type *i* generated within a region is determined to match the local density and molar fraction x_i:

$$N = \text{floor}\left(\frac{\rho \Delta x \Delta y \Delta z}{\bar{m}} x_i\right) \tag{2.13}$$

where Δx, Δy, and Δz are dimensions of the region and $\bar{m}$ is the average atomic mass given by:

$$\bar{m} = \sum_i x_i m_i \tag{2.14}$$

2.3.1 Positioning

Every generated atom within the MD simulation is given a unique Cartesian coordinate; determining its position within the simulation's box. The initial position of the atoms for a monatomic gas is simply generated by a uniform random number as shown below:

$$x = (x_{max} - x_{min})\xi + x_{min} \tag{2.15a}$$

$$y = (y_{max} - y_{min})\xi + y_{min} \tag{2.15b}$$

$$z = (z_{max} - z_{min})\xi + z_{min} \tag{2.15c}$$

The values *x*, *y*, *z* are the Cartesian coordinates, ξ is a uniform random number from the distribution $\xi \in [0, 1]$, and the *max* and *min* of *x*, *y*, and *z* are the maximum and minimum boundaries of the domain where the atom can be placed. This method occasionally leads to accidental overlaps of two or more atoms with nearly the same positions. As discussed earlier in Section 2.1, an energy minimization routine is used to separate overlapped atoms.

Diatomic molecules are positioned similarly, where first the geometric center of the molecule is positioned randomly within a given domain:

$$x_{center} = (x_{max} - x_{min})\xi + x_{min} \tag{2.16a}$$

$$y_{center} = (y_{max} - y_{min})\xi + y_{min} \tag{2.16b}$$

$$z_{center} = (z_{max} - z_{min})\xi + z_{min} \tag{2.16c}$$

The values x_{center}, y_{center}, and z_{center} are the Cartesian coordinates of the geometric center of the diatomic molecule. The molecule is then assigned a spherical orientation and the two atoms comprising the diatomic molecule are given appropriate Cartesian coordinates. This is pictured below in spherical coordinates.

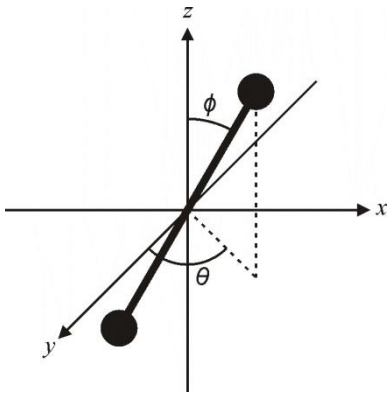

Figure 2.2: Orientation of Diatomic Molecule in Spherical Coordinates.

The positions of the two atoms relative to their geometric center are given by the following equations:[10]

$$x_{1,2} = x_{center} \pm \frac{r_0}{2}\sqrt{1-u^2}\cos\theta \tag{2.17a}$$

$$y_{1,2} = y_{center} \pm \frac{r_0}{2}\sqrt{1-u^2}\sin\theta \tag{2.17b}$$

$$z_{1,2} = z_{center} \pm \frac{r_0}{2}u \tag{2.17c}$$

$$u \equiv \cos\phi \tag{2.17d}$$

The values $x_{1,2}$, $y_{1,2}$ and $z_{1,2}$ are the Cartesian coordinates of the atoms comprising the diatomic molecule, where the subscripts represent each respective atom. For a linear diatomic molecule, the plus sign is for atom one and the negative sign is for atom two. The value r_0 is the equilibrium length of the diatomic molecule and represents the state in which the molecule has the maximum amount of kinetic vibrational energy. To ensure that the orientation of the molecule is uniformly distributed, θ is chosen from the uniform distribution $\theta \in [0, 2\pi)$ and $u \in [-1, 1]$. The value *u* is chosen randomly instead of $\phi \in [0, \pi]$ to prevent an uneven distribution of orientations towards $\phi = 0$ and π which would otherwise occur.

2.3.2 Atomic Translation Velocity

In addition to a predefined position, each atom requires an initial 3-dimensional velocity vector. For a monatomic gas this requires only a translational velocity and bulk velocity of the fluid. The bulk velocity is the average velocity of the fluid within the simulation. In general, for any simulated shock wave the bulk velocity is one dimensional; and in the cases presented here they are positive along the x-directional vector. The bulk velocity *U* of a fluid is calculated using the speed of sound *a*, and the Mach number *M*, of the fluid at a given state:

$$U = aM \tag{2.18}$$

where *a* is approximated using the Newton-Laplace equation for an ideal gas:[11]

$$a = \sqrt{\frac{\gamma RT}{\bar{M}}} \tag{2.19}$$

The value γ is the heat capacity ratio, *R* is the universal gas constant, and $\bar{M}$ is the average molar mass. Assuming an ideal gas, the heat capacity ratio γ is related to the degrees of freedom *f* present:[12]

$$\gamma = \frac{f + 2}{f} \tag{2.20}$$

For a monatomic gas, only three degrees of freedom are present. For a single species gas, the average molar mass is simply the molar mass of the species. However, for a mixed gas with multiple species, the average molar mass is given by the summation of the product of individual mole fractions, x_i, and molar masses, M_i:

$$\bar{M} = \sum_i x_i M_i \tag{2.21}$$

The translational velocity follows the standard Maxwellian distribution: [13]

$$\phi(v_{x,y,z}) = \left(\frac{m}{2\pi k_B T}\right)^{1/2} \exp\left[-\frac{m}{2k_B T} {v_{x,y,z}}^2\right] \tag{2.22}$$

For the function $\phi(v_{x,y,z})$, the value $v_{x,y,z}$ represents the velocity of the atom, while the subscript indicates the velocity component. The other values include *m*, the mass of the atom; k_B, Boltzmann's constant; and *T*, the temperature of the gas. In order to generate this distribution, a random number generator is used which follows a standard normal distribution, whose function is shown below:[14]

$$\phi(\chi) = \frac{1}{\sqrt{2\pi}} \exp\left[-\frac{1}{2}x^2\right] \tag{2.23}$$

Comparing Equation 2.22 and 2.23, the following relation can be reached:

$$\chi = \sqrt{\frac{m}{k_B T}} v_{x,y,z} \tag{2.24}$$

where χ is the standard normal distributed random number. From this relation, the translational velocity of a monatomic gas can be generated using the following equations:

$$v_x = \sqrt{\frac{k_B T}{m}} \chi + U \tag{2.25a}$$

$$v_y = \sqrt{\frac{k_B T}{m}} \chi \tag{2.25b}$$

$$v_z = \sqrt{\frac{k_B T}{m}} \chi \tag{2.25c}$$

2.3.3 Diatomic Vibrational Velocity

For a diatomic molecule, both atoms require individual velocity vectors. In addition to a bulk velocity and translational velocity component, an additional vibrational and rotational velocity component is required. The method for finding the bulk velocity and translational velocity of a monatomic gas may also be applied to a diatomic gas where the mass, *m*, and the average molar mass, $\bar{M}$, are the total mass and total molar mass of the molecule respectively. At low temperatures, where the vibrational component of a diatomic molecule can be neglected, $f = 5$. At higher temperatures, where the vibrational component cannot be neglected, $f = 6$. This is because, assuming distinct vibrational energy states, at low temperatures the energy needed to leave the ground vibrational state far exceeds the energy corresponding to the ambient temperature given by $k_B T$, and therefore does not significantly contribute to the heat capacity of the system. In general, the vibrational component can be neglected when the vibrational temperature of the molecule Θ_v is much less than the ambient temperature of the system. The vibrational temperature of Nitrogen is 3374 K.[15] While the vibrational temperature of a molecule can be found in many tables, it is defined by:[16]

$$\Theta_v \equiv \frac{h\nu}{k_B} \tag{2.26}$$

$$\nu = \frac{\sqrt{k/\mu}}{2\pi} \tag{2.27}$$

where h is the Planck constant, k is the force constant of the molecule, and μ is the molecule's reduced mass, defined by the summation:

$$\frac{1}{\mu} = \sum_i \frac{1}{m_i} \tag{2.28}$$

where m_i are the molecules' individual atomic masses.

Assuming the ambient temperature of the system is sufficient to excite the molecule's vibrational energy states, the probability, f_n, of the molecule being in a given discrete energy state is given by:[16]

$$f_n = \left(1 - e^{-\Theta_v/T}\right)e^{-n\Theta_v/T} \tag{2.29}$$

where n is the vibrational energy state. A vibrational velocity distribution can be generated from this function. By assigning each vibrational energy state a number equal to the summation of its probability and all probabilities of lower vibrational states,

$$P_v(n) = \sum_{i=0}^{n} f_n(i) \tag{2.30}$$

a random energy state can be selected with the correct distribution using a uniform random number from the distribution $\xi \in [0, 1]$. If this uniform random number is less than $P_v(n)$, but greater than $P_v(n-1)$, then the energy state, n, is selected. From this

energy state, the total vibrational energy, ε_v, of the molecule is given by:

$$\varepsilon_v = \left(n + \frac{1}{2}\right)\Theta_v k_B \tag{2.31}$$

While the MD simulation is classical in nature, when given a high ambient temperature, a distribution based on discrete energy levels is sufficient to populate the simulation, assuming there are a sufficient number of molecules to populate the energy states above the ground state.

Assuming the diatomic molecule acts as a classical spring, given the total vibrational energy of a molecule and the force constant *k*, the maximum displacement Δr_{max} that the molecule is allowed to stretch or compress beyond the equilibrium length r_0 is given by:

$$\Delta r_{max} = \sqrt{\frac{2\varepsilon_v}{k}} \tag{2.32}$$

Because a spring's movement is sinusoidal relative to the linear movement of time, the actual displacement Δr is determined using the formula below:

$$\Delta r = \Delta r_{max} \cos(\pi \cdot \xi) \tag{2.33}$$

where ξ is a uniform random number from the distribution $\xi \in [0, 1]$. Given this

displacement, the vibrational potential energy, PE_v, of the molecule is given by:

$$PE_v = \frac{1}{2} k \Delta r^2 \tag{2.34}$$

The vibrational kinetic energy of each atom is then:

$$KE_{v_1} = \frac{\varepsilon_v - PE_v}{1 + \frac{m_1}{m_2}} \tag{2.35a}$$

$$KE_{v_2} = \frac{\varepsilon_v - PE_v}{1 + \frac{m_2}{m_1}} \tag{2.35b}$$

where the values m_1 and m_2 are the masses of each individual atom.

The vibrational speed, $v_{v_{1,2}}$, of each atom is then:

$$v_{v_{1,2}} = \pm b \sqrt{\frac{2KE_{v_{1,2}}}{m_{1,2}}} \tag{2.36}$$

where *b* is a randomly assigned number that can be either -1 or 1 to indicate whether the molecule is expanding or contracting. In order to add the vibrational velocity and displacement components to the current state of the molecule, the normal vector along the molecular axis is needed. The distance between the two atoms, *r*, comprising the

diatomic molecule is given by:

$$r = \sqrt{(x_2 - x_1)^2 + (y_2 - y_1)^2 + (z_2 - z_1)^2} \tag{2.37}$$

where *x*, *y* and *z* are the spatial coordinates of each atom. The normal vector (n_x, n_y, n_z) along the molecular axis is then:

$$n_x = \frac{x_2 - x_1}{r} \tag{2.38a}$$

$$n_y = \frac{y_2 - y_1}{r} \tag{2.38b}$$

$$n_z = \frac{z_2 - z_1}{r} \tag{2.38c}$$

Given the normal vector, (n_x, n_y, n_z), the vibrational velocity of each atom can then be added to their exciting velocity components, as shown below:

$$v_{x_{1,2}} = v^*_{x_{1,2}} + n_x v_{v_{1,2}} \tag{2.39a}$$

$$v_{y_{1,2}} = v^*_{y_{1,2}} + n_y v_{v_{1,2}} \tag{2.39b}$$

$$v_{z_{1,2}} = v^*_{z_{1,2}} + n_z \, v_{v_{1,2}} \tag{2.39c}$$

The asterisk indicated the atom's previous state before the vibrational components were added.

In order to account for the vibrational potential energy, the atoms are then displaced from their original positions. The individual displacement of each atom from their original position is given by:

$$\Delta r_1 = \frac{r_0 + \Delta r - r}{1 + \frac{m_1}{m_2}} \tag{2.40a}$$

$$\Delta r_2 = \frac{r_0 + \Delta r - r}{1 + \frac{m_2}{m_1}} \tag{2.40b}$$

Using the normal vector, (n_x, n_y, n_z), the atom's new spatial coordinates are then:

$$x_{1,2} = x^*_{1,2} \mp n_x \Delta r_{1,2} \tag{2.41a}$$

$$y_{1,2} = y^*_{1,2} \mp n_y \Delta r_{1,2} \tag{2.41b}$$

$$z_{1,2} = z^*_{1,2} \mp n_z \Delta r_{1,2} \tag{2.41c}$$

As before, the asterisk indicated the atom's previous state before the vibrational components were added.

While using discrete quantum energy states to populate a classical MD simulation is acceptable within high ambient temperatures, it is inadequate for ambient temperatures which are much less than the vibrational temperature Θ_v. At low ambient temperatures, using discrete energy states, virtually all molecules are in the ground state. Furthermore, according to Equation 2.31, even in a ground state, a molecule physically has a minimum vibrational energy that can never be lost. However, in a classical MD simulation there is nothing preventing energy from being transferred out of or into the vibrational state at any temperature. As a result, in a classical MD simulation, if the minimum ground state energy is applied to all ground state molecules, part of that energy would be transferred into other forms of energy, including translational and rotational energy. This would unrealistically increase the temperature of the system. In the same sense, a system whose molecules are predominantly in the ground state and given no vibrational energy would unrealistically absorb energy, thus decreasing the temperature of the system. In order to solve this, for a system whose ambient temperature is much less than the vibrational temperature, all molecules are assigned a vibrational energy given by the kinetic theory of an ideal gas:[16]

$$\varepsilon_v = k_B T \tag{2.42}$$

While distribution of vibrational energies will eventually develop in a classical MD

simulation over time, the total vibrational energy will remain constant. Alternatively, if it is known that the entire system will have an ambient temperature well below the vibrational temperature, it is possible to simulate the molecules as vibrationally rigid by fixing the bond length between atoms to the equilibrium bond distance using the *shake* algorithm, outlined previously in Section 2.1. However, this method is not always possible depending on the simulation.

2.3.4 Diatomic Rotational Velocity

The rotational velocity component for a diatomic molecule is found in much the same way as the vibrational component using discrete energies. The probability f_J of the molecule being in a given rotational energy state is given by:[16]

$$f_J = (2J+1)(\Theta_r/T)e^{-\Theta_r J(J+1)/T} \tag{2.43}$$

where J is the rotational energy state, Θ_r is the rotational temperature, and T is the ambient temperature. The rotational temperature for Nitrogen is 2.88 K.[15] The definition of rotational temperature is:[16]

$$\Theta_r \equiv \frac{hB}{k_B} \tag{2.44}$$

$$B = \frac{h}{8\pi^2 I} \tag{2.45}$$

where *I* is the moment of inertia of the molecule. Using Equation 2.43, a random rotational distribution can be assigned to each molecule. Giving each rotational energy state a number equal to the summation of its probability and all probabilities of lower rotational states:

$$P_r(J) = \sum_{i=0}^{J} f_J(i) \tag{2.46}$$

a random energy state can then be selected with the correct distribution using a uniform random number from the distribution $\xi \in [0, 1]$. If this uniform random number is less than $P_r(J)$, but greater than $P_r(J-1)$, then the energy state, *J*, is selected. From this energy state, the total rotational energy, ε_r, of the molecule is given by:[16]

$$\varepsilon_r = \Theta_r k_B J(J+1) \tag{2.47}$$

The rotational energy is then divided between each atom of the diatomic molecule based on their relative masses, m_1 and m_2.

$$KE_{r_1} = \frac{\varepsilon_r}{1 + \frac{m_1}{m_2}} \tag{2.48a}$$

$$KE_{r_2} = \frac{\varepsilon_r}{1 + \frac{m_2}{m_1}} \tag{2.48b}$$

The additional rotational speed, $v_{r_{1,2}}$, added to each atom is then:

$$v_{r_{1,2}} = \sqrt{\frac{2KE_{r_{1,2}}}{m_{1,2}}} \tag{2.49}$$

This rotational speed can then be added to the diatomic molecule's existing velocity given the normal vector along the axis of the molecule described in Equation 2.38 and a random normal vector perpendicular to the molecular axis. In order to create a random normal vector perpendicular to the molecular axis, a reference perpendicular vector $\boldsymbol{a}$ is used. Using the dot product and assuming the *x* and *y* components of the reference vector are one, this vector is defined as:

$$a_x = 1 \tag{2.50a}$$

$$a_y = 1 \tag{2.50b}$$

$$a_z = -\frac{n_x + n_y}{n_z} \tag{2.50c}$$

where n_x, n_y, and n_z are the normal vectors along the molecular axis. The length of

vector $\boldsymbol{a}$ and its normal vector, $\boldsymbol{n}_a$, is then:

$$|\boldsymbol{a}| = \sqrt{2 + {a_z}^2} \tag{2.51}$$

$$n_{a_x} = \frac{1}{|\boldsymbol{a}|} \tag{2.52a}$$

$$n_{a_y} = \frac{1}{|\boldsymbol{a}|} \tag{2.52b}$$

$$n_{a_z} = \frac{a_z}{|\boldsymbol{a}|} \tag{2.52c}$$

A random orientation θ between vectors $\boldsymbol{n}_a$ and the normal rotational vector $\boldsymbol{n}_r$ is chosen from a uniform random number from the distribution $\theta \in (0, 2\pi)$. Using the cross product between these two vectors the normal rotational vector is given by:

$$n_{r_x} = \frac{-b + \sqrt{b^2 - 4c}}{2} \tag{2.53a}$$

$$b = 2 \sin\theta \left(n_{a_y} n_z - n_{a_z} n_y \right) \tag{2.53b}$$

$$c = \sin^2\theta \left({n_z}^2 + {n_y}^2 \right) - {n_{a_x}}^2 \tag{2.53c}$$

$$n_{r_y} = \frac{n_{a_y} n_{r_x} + n_z \sin\theta}{n_{a_x}} \tag{2.53d}$$

$$n_{r_z} = \frac{n_{a_z} n_{r_x} - n_y \sin\theta}{n_{a_x}} \tag{2.53e}$$

From the rotational vector $\boldsymbol{n}_r$ the rotational speeds $v_{r_{1,2}}$ for each atom can be added to their previous velocities, $\boldsymbol{v}^*_{1,2}$:

$$v_{x_{1,2}} = v^*_{x_{1,2}} \pm n_{r_x} v_{r_{1,2}} \tag{2.54a}$$

$$v_{y_{1,2}} = v^*_{y_{1,2}} \pm n_{r_y} v_{r_{1,2}} \tag{2.54b}$$

$$v_{z_{1,2}} = v^*_{z_{1,2}} \pm n_{r_z} v_{r_{1,2}} \tag{2.54c}$$

It is important to note that this method fails if the molecular axis $\boldsymbol{n}$ lies in or very near the *xy*-plane. Under these conditions the reference vector $\boldsymbol{a}$ cannot be assumed to have components $a_x = 1$ and $a_y = 1$, because, if $n_z \approx 0$, component a_z would approach infinity. In C++ this produces a non-existent number *NaN*. If this occurs, the procedure is repeated with the revised assumptions that $a_x = 0$, $a_y = 0$ and $a_z = 1$. This ensures the reference vector $\boldsymbol{a}$ is perpendicular to any vector within the *xy*-plane.

2.4 Sampling Methods

Once a simulation has been sufficiently evolved in time to reach steady state, the atoms within the simulation are sampled and binned to determine local densities, velocities and energies. This typically occurs around 1.5×10^7 time steps or 50 mean collision times from $t = 0$. The simulation is then sampled at a rate of Δt and averaged over all samples. To save computer memory, the position and velocity of every atom for every sample is not recorded. Instead, the atoms' positions and velocities are sorted into bins and averaged together with previous samples to be post-processed at a later time. A bin consists of a specified range of values which defines the number of data points or "resolution" of a simulation to which it can be analyzed. The resolution of these bins are not strictly calculated, but rather intuitively chosen to provide an acceptable compromise between the resolution of a simulation and the number of samples that are needed to produce a consistent average within that bin. If the bin size is too small, not enough particles will satisfy that condition within a reasonable number of sample periods, leading to a widely fluctuating average from one bin to another.

Because LAMMPS is a massively parallel program, each processor simulates the movement of a section of the simulation box. The atoms within each section are stored on the corresponding processor. To utilize the parallel nature of LAMMPS and increase the rate at which a simulation can be sampled, each processor only samples the atoms to which it is assigned by LAMMPS. These local averaged samples are then combined at a later time.

For monatomic gas the atoms' positions and velocities can be passed from LAMMPS to a sampling routine and immediately binned. However, for a diatomic gas, molecular bonds must first be identified, associating a pair of atoms with a molecule. If a bond style such as a harmonic bond is used to simulate the bond interaction between two atoms, LAMMPS will already contain a list of bonds associated with each atom. In this case this information can be used by the sampling routine. If, however, only a pair style such as a Lennard-Jones potential is used to simulate the inter-atomic potential between atoms including bond interaction, LAMMPS will store a list of which atoms are bonded to each other. In this case, the sampling routine must identify bonded atoms. Currently, this is done by calculating the distance between every atom being sampled. If the distance between two atoms is within a specified bond cutoff distance r_c, the atoms are considered to be bonded. While it is possible that two colliding atoms could be within the value of r_c, it is generally considered that this will be a relatively rare condition in the assumed ideal non-interacting gas of the simulation and therefore will not contribute to the overall average of the properties being measured. Using this current method results in $O(n^2)$ calculations per processor. Due to the parallel nature of LAMMPS, occasionally the atoms of a molecule will be split between two or more processors and the atoms bordering the domain of one processor will generally interact with atoms on another. To maintain these interactions, LAMMPS stores on each processor a copy of the position and velocity of "ghost" atoms which border the domain of that processor. While the movements of these ghost atoms are static, they are used to simulate the movement of the atoms within the processor's domain. These ghost atoms can also be accessed by the

sampling routine to reconstruct molecules split between two processors. To prevent double counting of these molecules, once on one processor and once on the other, the sampling routine compares the ID number associated with each atom. Only the processor containing the largest atomic ID number of the molecule in question, that is not a ghost atom, samples that molecule.

2.4.1 Local Density

Once all particles are identified, they are sorted by species and binned by their spatial placement within the simulation. Because the shock wave is only one dimensional along the flow of the fluid, the properties of the shock wave only vary in the x-direction. Therefore, only the x-component of an atom's position is used to spatially bin the particle. The typical length of a spatial bin size used in these simulations was 300 angstrom, or roughly 0.2% to 0.5% of the total length of the simulation box. However, a more standardized bin size of 0.1 inflow mean free paths, $\lambda_{1,}$ was used by Matsumoto in his simulations.[6] On average this provided the necessary balance between resolution and sampling duration. For a polyatomic molecule, the position of the center of mass x_c is used to determine the bin into which it would be placed:

$$x_c = \frac{\sum_i x_i m_i}{\sum_i m_i} \tag{2.55}$$

where x_i and m_i are the x-coordinate and mass, respectively, of each atom within a particle.

All properties of the fluid are per individual bin and are derived based only on the particles placed in those bins. A sum of particles sorted by species and spatial placement is recorded and later processed to provide a number density, ρ_n, of each species and bin:

$$\rho_n = \frac{n}{\Delta x(y_{max} - y_{min})(z_{max} - z_{min})} \tag{2.56}$$

where *n* is the number of particles of a given species in a given bin, Δx is the length of a bin, and y_{max}, y_{min}, $z_{max}$and z_{min} are the maximum and minimum domains of the simulation box in the *y* and *z* direction respectively.

2.4.2 Translational Properties

A particle's translational velocity, $\boldsymbol{v}_{tr}$, through the fluid is given by taking the weighted average of each atom's velocity making up the particle:

$$v_{tr_x} = \frac{\sum_i v_{x_i} m_i}{\sum_i m_i} \tag{2.57a}$$

$$v_{tr_y} = \frac{\sum_i v_{y_i} m_i}{\sum_i m_i} \tag{2.57b}$$

$$v_{tr_z} = \frac{\sum_i v_{z_i} m_i}{\sum_i m_i} \tag{2.57c}$$

The particle's translational velocity and translational velocity squared are then summed respectively with that of all other particles of the same species. The sum of translational velocities and velocities squared are later post-processed to find the average velocity of the fluid and parallel, perpendicular and overall translational temperatures of a given bin and species. The average velocity, $\boldsymbol{V}$, of a species is simply the sum of translational velocities $\sum_n \boldsymbol{v}$ divided by the sum of particles of that species *n*. The translational temperature which is derived from the speed of a particle relative to the velocity of flow is then given by:

$$T_{tr} = \frac{m}{3k_B n}\left[\sum_n \left({v_{tr_x}}^2 + {v_{tr_y}}^2 + {v_{tr_z}}^2\right) - \frac{\left(\sum_n v_{tr_x}\right)^2 + \left(\sum_n v_{tr_y}\right)^2 + \left(\sum_n v_{tr_z}\right)^2}{n}\right] \tag{2.58}$$

where *m* is the atomic mass of the species. The parallel temperature, $T_{\parallel}$, and perpendicular temperature, $T_{\perp}$, are the components of the translational temperature due to the velocity of the particle parallel to the flow and perpendicular to the flow, respectively:

$$T_{\parallel} = \frac{m}{k_B n}\left[\sum_n {v_{tr_x}}^2 - \frac{\left(\sum_n v_{tr_x}\right)^2}{n}\right] \tag{2.59}$$

$$T_{\perp} = \frac{m}{2k_B n}\left[\sum_n \left({v_{tr_y}}^2 + {v_{tr_z}}^2\right) - \frac{\left(\sum_n v_{tr_y}\right)^2 + \left(\sum_n v_{tr_z}\right)^2}{n}\right] \tag{2.60}$$

Besides temperature, the translational velocity also provides information about the velocity distribution of a species at a given location within a shock wave. A velocity distribution function represents the probability of a particle falling within a range of velocities. To analyze this, particles are sorted by velocity into "bins" which sum the number of particles that fall within a given range of velocities, Δv. As with spatial bins, the span of these velocity bins are chosen to provide an adequate balance between resolution and the number of samples required to produce a consistent average. As velocities in these simulations can range from several hundred to several thousand meters per second, a velocity bin size of 50 angstroms was generally chosen for all simulations. A sum of the number of particles that fall into a velocity bin β_i is then later used to produce a plot of the velocity distribution function $\phi(v_x)$ for that species:

$$\phi([i + 1/2]\Delta v) = \frac{\beta_i}{n\Delta v} \tag{2.61}$$

where the bin index *i* can range from -∞ to ∞ in increments of 1 and *n* is the total number of particles sampled over all velocity bins, $n = \sum_{i=-\infty}^{\infty} \beta_i$, which is also the total number of particles sampled in a given spatial bin. Similarly, this method can be applied to velocities' components in the *y* and *z* direction.

2.4.3 Vibrational and Rotational Energy

For a diatomic particle, additional vibrational and rotational components of the particle's velocity must be considered. By subtracting the translational velocity of the particle, $\boldsymbol{v}_{tr}$, given by Equation 2.57 from the velocity of each atom, $\boldsymbol{v}_{1,2}$, only the components of velocity due to vibration and rotation, $\boldsymbol{v}_{vib,rot}$, are left. The vibrational component of $\boldsymbol{v}_{vib,rot}$ is given by the projection of the velocity vector, $\boldsymbol{v}_{vib,rot}$, along the molecular axis of the molecule $\Delta\boldsymbol{x}$ which is given by the position of the two atoms:

$$\Delta x = x_2 - x_1 \tag{2.62a}$$

$$\Delta y = y_2 - y_1 \tag{2.62b}$$

$$\Delta z = z_2 - z_1 \tag{2.62c}$$

The vibrational velocity $\boldsymbol{v}_{vib}$ of each atom is then:

$$v_{vib_{x_{1,2}}} = \frac{v^*_{x_{1,2}}\Delta x + v^*_{y_{1,2}}\Delta y + v^*_{z_{1,2}}\Delta z}{\Delta x^2 + \Delta y^2 + \Delta z^2}\Delta x \tag{2.63a}$$

$$v_{vib_{y_{1,2}}} = \frac{v^*_{x_{1,2}}\Delta x + v^*_{y_{1,2}}\Delta y + v^*_{z_{1,2}}\Delta z}{\Delta x^2 + \Delta y^2 + \Delta z^2}\Delta y \tag{2.63b}$$

$$v_{vib_{z_{1,2}}} = \frac{v^*_{x_{1,2}}\Delta x + v^*_{y_{1,2}}\Delta y + v^*_{z_{1,2}}\Delta z}{\Delta x^2 + \Delta y^2 + \Delta z^2}\Delta z \tag{2.63c}$$

where $\boldsymbol{v}^* = \boldsymbol{v}_{vib,rot}$.

Given the distance between the atoms, $r = |\Delta \boldsymbol{x}|$, or from Equation 2.37, the vibrational energy, ε_{vib}, of the diatomic molecule is then given by the sum of kinetic energy due to the vibrational velocity and potential energy due to the force exerted between the two atoms:

$$\varepsilon_{vib} = \underbrace{\frac{1}{2}\left[m_1\left({v_{vib_{x_1}}}^2 + {v_{vib_{y_1}}}^2 + {v_{vib_{z_1}}}^2\right) + m_2\left({v_{vib_{x_2}}}^2 + {v_{vib_{y_2}}}^2 + {v_{vib_{z_2}}}^2\right)\right]}_{Kinetic\ Energy} + \underbrace{\frac{1}{2}K(r - r_0)^2}_{Potential\ Energy} \tag{2.64}$$

where m_1 and m_2 are the masses of each atom, k is the force constant between the atoms and r_0 is the equilibrium length of the molecule. The vibrational energy is then summed with the vibrational energy of all other sampled particles of the same species, $\sum_n \varepsilon_v$, which is then used to find the classical vibrational temperature of the fluid:[13]

$$T_{vib} = \frac{\sum_n \varepsilon_{vib}}{k_B n} \tag{2.65}$$

While the MD simulation performed by LAMMPS is classical in nature, a vibrational energy state can be estimated from the vibrational energy. This allows us to see how well the vibrational energy distribution developed by a classic MD simulation compares to that described by a discrete quantum energy states distribution. Using Equations 2.31, the vibrational energy state, *n*, of the particle is given by the truncation of:

$$n = \text{trunc}\left(\frac{\varepsilon_{vib}}{\Theta_{vib} k_B} - \frac{1}{2}\right) \tag{2.66}$$

The value is truncated rather than rounded so as to say that a vibrational energy state can only be reached given a minimum amount of energy. All particles sampled in a given energy state, *n*, are summed together and then divided by the total number of particles to provide a vibrational energy distribution.

Given the translational velocity, $\boldsymbol{v}_{tr}$, from Equation 2.57 and vibrational velocity, $\boldsymbol{v}_{vib}$, from Equation 2.63, the remaining rotational velocity, $\boldsymbol{v}_{rot}$, of each atom within a diatomic molecule is simply:

$$v_{rot_{x_{1,2}}} = v_{x_{1,2}} - v_{tr_x} - v_{vib_{x_{1,2}}} \tag{2.67a}$$

$$v_{rot_{y_{1,2}}} = v_{y_{1,2}} - v_{tr_y} - v_{vib_{y_{1,2}}} \tag{2.67b}$$

$$v_{rot_{z_{1,2}}} = v_{z_{1,2}} - v_{tr_z} - v_{vib_{z_{1,2}}} \tag{2.67c}$$

The total rotational energy of the particle is then given by the kinetic energy of each atom based on their rotational velocities respectfully:

$$\varepsilon_{rot} = \frac{1}{2} m_1 \left({v_{rot_{x_1}}}^2 + {v_{rot_{y_1}}}^2 + {v_{rot_{z_1}}}^2 \right) + \frac{1}{2} m_2 \left({v_{rot_{x_2}}}^2 + {v_{rot_{y_2}}}^2 + {v_{rot_{z_2}}}^2 \right) \tag{2.68}$$

The rotational energy is then summed with the rotational energy of all other sampled particles of the same species, $\sum_n \varepsilon_v$, which is then used to find the classical rotational temperature of the fluid:[13]

$$T_{rot} = \frac{\sum_n \varepsilon_{rot}}{k_B n} \tag{2.69}$$

As with the vibrational energy, the rotational energies of the particles can be sorted into discrete energy states. Using Equation 2.47, the discreet rotational energy state of a particle given, ε_{rot}, is:[17]

$$J = \text{trunc} \left(\frac{1}{2} \left[-1 + \sqrt{1 + 4 \frac{\varepsilon_{rot}}{\Theta_{rot} k_B}} \right] \right) \tag{2.70}$$

All particles sampled in a given energy state, *J,* are summed together and then divided by the total number of particles to provide a rotational energy distribution. Additionally, rotational and vibrational energies can be binned similarly to the translational velocity without the need to determine a quantum energy state.

3 Results and Discussion

In order to gauge the accuracy of MD within a highly non-equilibrium system, shock wave structures composed of Helium-Argon, Helium-Xenon, and diatomic Nitrogen were simulated by MD and compared to experimental results and DSMC simulations. These include experimental results by Harnett and Muntz[1] for Helium-Argon, Germanized Hard-Sphere (GHS) DSMC simulations by Hassan and Hash[5] for Helium-Argon and Helium-Xenon, Hard Sphere DSMC simulations by Brid[4], and experimental results by Robben and Talbot.[2]

3.1 Experimental Comparison of Helium-Argon Gas Mixtures

Experimental results by Harnett and Muntz[1] measured using an electron beam fluorescence technique included shock structures composed of 11.5% Argon-88.5% Helium, 24.7% Argon-75.3% Helium, and 44% Argon-56% Helium. The Mach numbers and inflow free stream temperatures for these cases are 1.58 and 162.5 K, 1.63 and 156.5 K, and 1.65 and 154.4 K, respectively. Velocity profiles for Argon and Helium are shown in Figures 3.1 through 3.3 and Argon, Helium, and mean temperature profiles are shown in Figures 3.4 through 3.12 for each case respectively. The agreement between MD and experimental profiles for velocity are excellent while agreement between temperature profiles is less agreeable. In all cases the MD inflow and outflow temperatures were higher than those shown in experiment. Despite this, the general separation trend for Helium parallel and perpendicular temperatures and Argon-Helium mean temperatures agree well, while MD parallel and perpendicular temperature trends for Argon are

opposite of those from experiment.

Inflow densities of 0.55 kg/m^3, 0.45 kg/m^3 and 0.5 kg/m^3 were chosen for the 11.5%, 24.7, and 44%-Argon cases, respectively. In general, inflow densities, ρ_1, were chosen to be as low as possible to be dilute, but high enough to be computationally tractable. However, as discussed in Section 2.2, the maximum length of the MD simulation domain was limited and therefore inflow densities were adjusted to fit the shock profile within the limited domain of the MD simulation. As discussed in Section 2.2, due to the dilute gas assumptions used to generate the atoms and the non-dilute nature of the gas at the densities assigned, the inflow and outflow conditions of the shock diverged from the set conditions. This resulted in an outflow temperature and density that was 1.1% hotter and 1.8% less dense for 11.5%-Argon, 1.0% hotter and 1.2% less dense for 24.7%-Argon, and 1.8% hotter and 1.8% less dense for 44%-Argon, than what was expected or enforced by the boundary conditions. It should also be noted that the shock profile simulated in MD for 11.5%-Argon, 24.7%-Argon, and 44%-Argon drifted towards the inflow by approximately 8, 10, and 5 bins, respectively, each bin being 300 Å long. The MD results were averaged over this drift resulting in a small smearing of the data.

A length scaling factor *L* was used to scale the MD profiles to the Harnett and Muntz data. This factor is described by:

$$L = \frac{\mu^*}{\rho_1 u_1} \tag{3.1}$$

Harnett and Muntz only indicate that the starred superscript indicates a sonic condition and therefore it is assumed that μ^* is the viscosity of the mixture at sonic conditions and ρ_1 and u_1 are the inflow density and velocity respectively.

Based on work from Robben and Talbot[2] in which a similar scaling factor was used, the temperature at sonic conditions T^* is described by[17]

$$T^* = \frac{2T_0}{\gamma + 1} \tag{3.2}$$

where γ is the heat capacity ratio for a monatomic gas and T_0 is the stagnation temperature of the flow given by:[17]

$$T_0 = T\left(1 + \frac{\gamma - 1}{2} {M_1}^2\right) \tag{3.3}$$

where M_1 is the pre-shock Mach number. The viscosity $\mu^*(T^*)$ is then readily obtained as described in Appendix A. For the MD simulations a length scale factor, *L*, of 397 Å for 11.5%-Argon, 624 Å for 24.7%-Argon, and 694 Å for 44%-Argon are used. The positioning of the shock along the *x*-axis was arbitrary and chosen to provide best fit. The experimental error in position reported by Harnett and Muntz was ±0.9 x/L.

The velocity profiles for 11.5%-Argon, 24.7%-Argon and 44%-Argon are shown below. The error in velocity for the experimental values was reported as $\pm 2 \times 10^3$ cm/s.

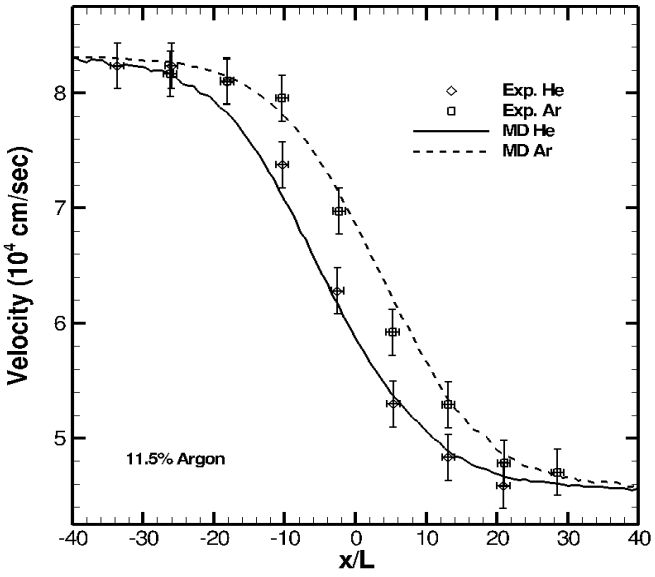

Figure 3.1: Velocity profiles of Argon (squares for experiment, dashed line for MD) and Helium (diamond for experiment, solid line for MD) for 11.5%-Argon mixture.

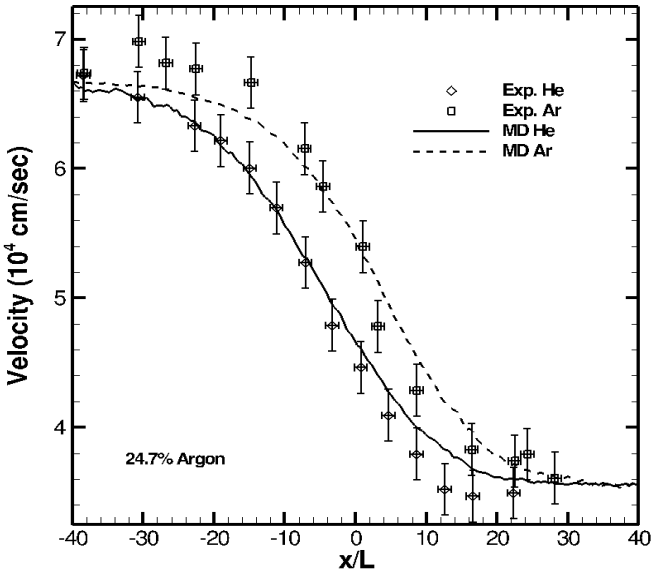

Figure 3.2: Velocity profiles of Argon (squares for experiment, dashed line for MD) and Helium (diamond for experiment, solid line for MD) for 24.7%-Argon mixture.

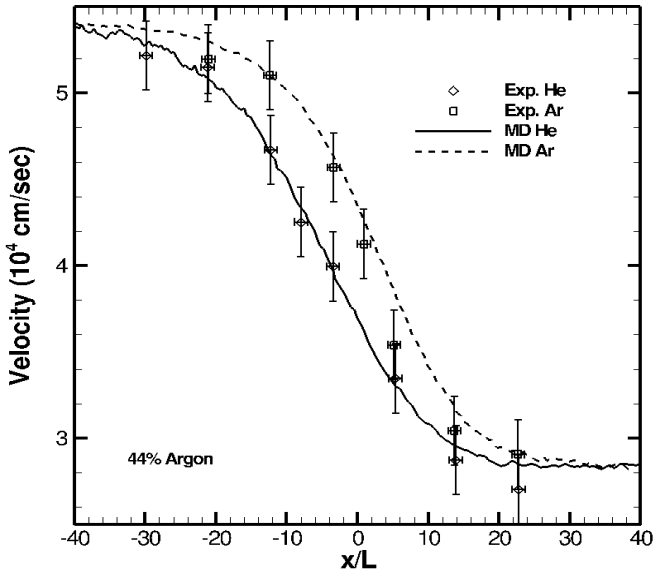

Figure 3.3: Velocity profiles of Argon (squares for experiment, dashed line for MD) and Helium (diamond for experiment, solid line for MD) for 44%-Argon mixture.

The agreement between velocity profiles is excellent with the exception of the 24.7%-Argon case in Figure 3.2. In this case the shock profile is slightly thicker, however, the separation trend between Argon and Helium velocity profiles still agrees well with the experiment. In all cases the Helium velocity profile develops before the Argon velocity profile as predicted by the experiment. It should be noted that the experimental Helium velocity profile for 24.7%-Argon was obtained indirectly by Harnett and Muntz from the density profile, which was not given, and converted to a velocity profile by the continuity equation.

Temperature profiles including parallel and perpendicular temperatures for Argon and Helium, and mean species temperatures are show in Figures 3.4 through 3.12. In all temperature profiles the estimated error reported by Harnett and Muntz for each case was

±4.6 K for 11.5%-Argon, ±4.5 K for 24.7%-Argon, and ±5.2 K for 44%-Argon. The parallel and perpendicular temperature profiles for Argon are shown below:

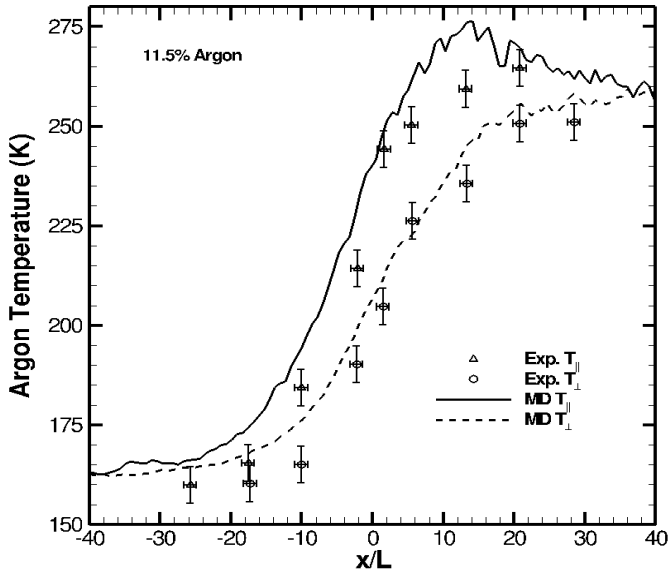

Figure 3.4: Perpendicular (circles for experiment, dashed line for MD) and parallel (triangle for experiment, solid line for MD) temperature profiles of Argon for 11.5%-Argon mixture.

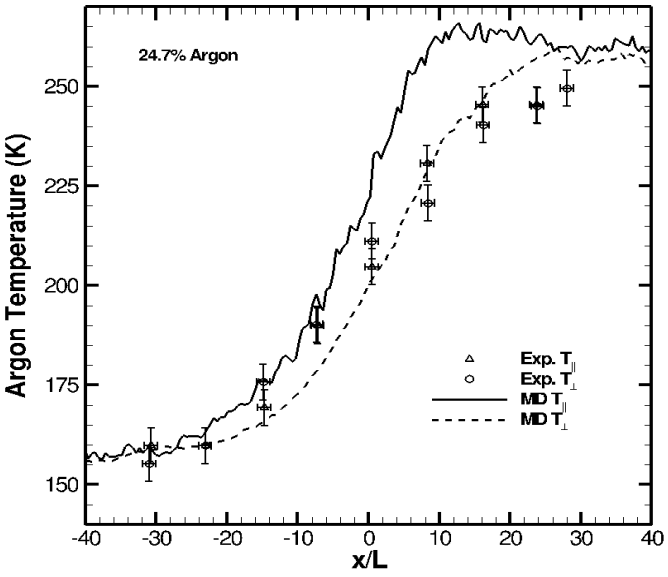

Figure 3.5: Perpendicular (circles for experiment, dashed line for MD) and parallel (triangle for experiment, solid line for MD) temperature profiles of Argon for 24.7%-Argon mixture.

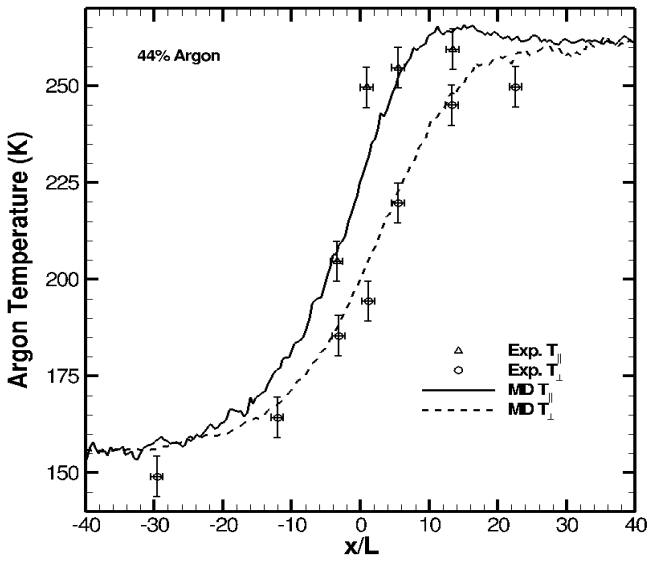

Figure 3.6: Perpendicular (circles for experiment, dashed line for MD) and parallel (triangle for experiment, solid line for MD) temperature profiles of Argon for 44%-Argon mixture.

For the 11.5%-Argon and 44%-Argon mixtures the MD trend between parallel and perpendicular temperatures agrees well with experimental results where the parallel temperature develops before the perpendicular temperature with a steeper slope and a slight temperature overshoot. While this trend is also observed in the 24.7%-Argon mixture for MD, it is not seen in the experimental results for that mixture. Harnett and Muntz theorized this lack of overshoot for the 24.7%-Argon case was caused, presumably, by an increase in cross collisions over the 44%-Argon case and the overshoot seen in the 11.5%-Argon case was due to uncertainty of the temperature measurement. In contrast, a temperature overshoot is predicted for each Argon-Helium mixture by MD simulation. Parallel and perpendicular temperature profiles of Helium are shown below:

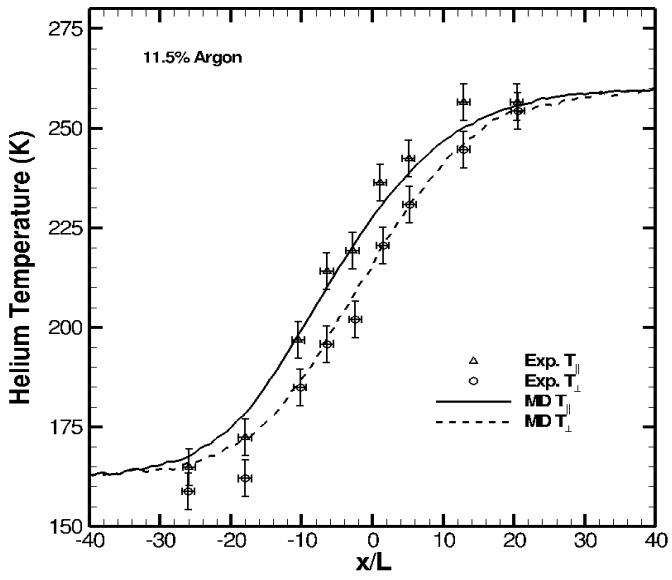

Figure 3.7: Perpendicular (circles for experiment, dashed line for MD) and parallel (triangle for experiment, solid line for MD) temperature profiles of Helium for 11.5%-Argon mixture.

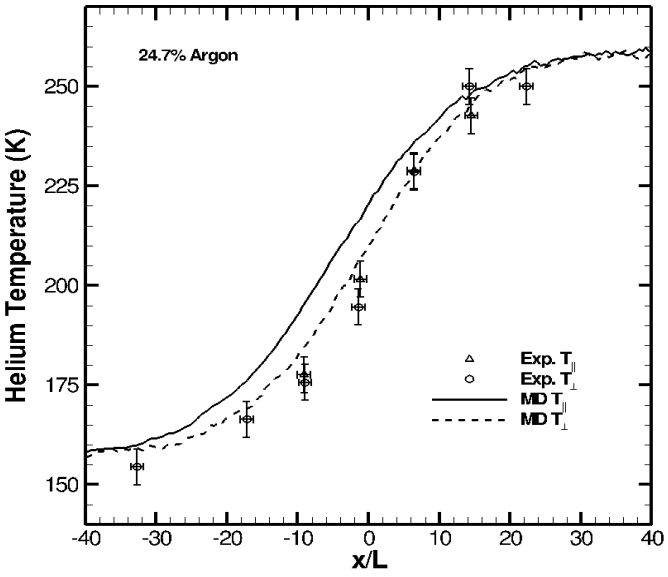

Figure 3.8: Perpendicular (circles for experiment, dashed line for MD) and parallel (triangle for experiment, solid line for MD) temperature profiles of Helium for 24.7%-Argon mixture.

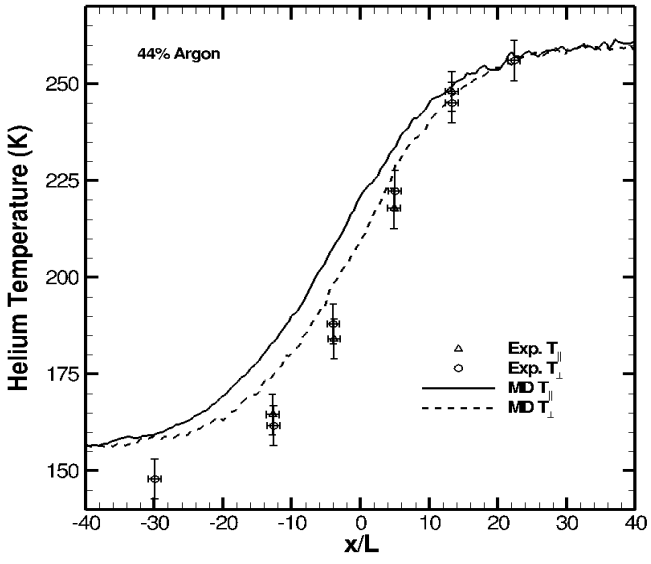

Figure 3.9: Perpendicular (circles for experiment, dashed line for MD) and parallel (triangle for experiment, solid line for MD) temperature profiles of Helium for 44%-Argon mixture.

The trend between parallel and perpendicular Helium temperatures for an 11.5%-Argon mixture agrees well between MD and experiment; however, any experimental trend for 24.7%-Argon or 44%-Argon is not visible due to experimental uncertainty. It was expected by Harnett and Muntz that as the fraction of Argon decreases, Helium would increasingly behave as a pure gas, resulting in an increased tendency for Helium to separate between parallel and perpendicular temperatures. While experimentally separation is only visible in the 11.5%-Argon case, it can be observed in all three MD cases with a general trend of increased separation between parallel and perpendicular Helium temperatures as the mole fraction of Helium increases. Finally, the mean temperature profiles for Argon and Helium for each case are shown below:

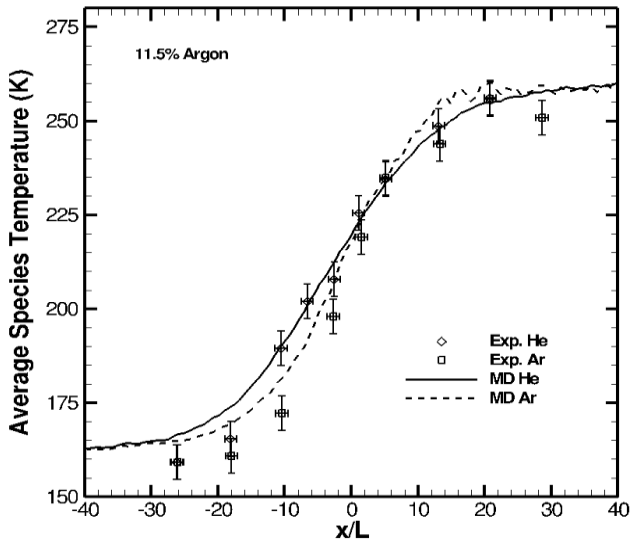

Figure 3.10: Average temperature profiles of Argon (squares for experiment, dashed line for MD) and Helium (diamond for experiment, solid line for MD) for 11.5%-Argon mixture.

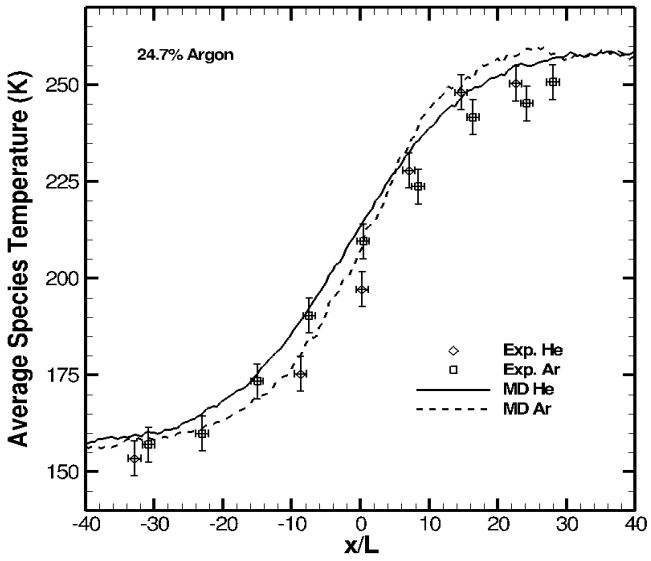

Figure 3.11: Average temperature profiles of Argon (squares for experiment, dashed line for MD) and Helium (diamond for experiment, solid line for MD) for 24.7%-Argon mixture.

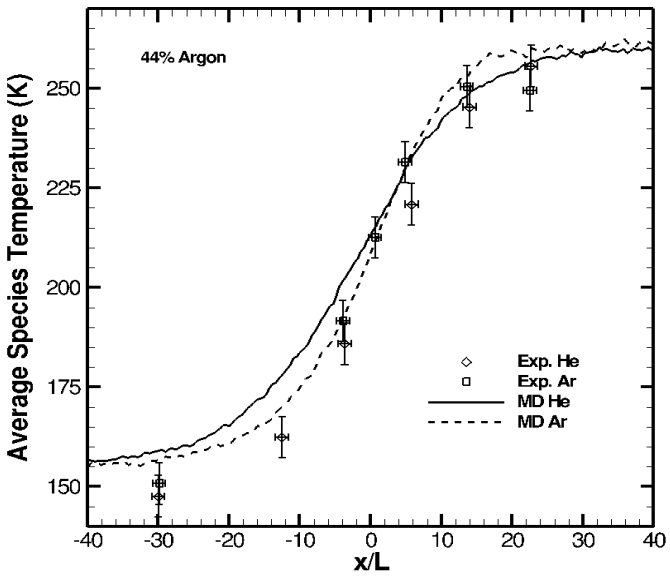

Figure 3.12: Average temperature profiles of Argon (squares for experiment, dashed line for MD) and Helium (diamond for experiment, solid line for MD) for 44%-Argon mixture.

Mean temperatures between Argon and Helium overall agree well between MD and experiment for all three cases. While not visible in the experimental data, Harnett and Muntz expected an overshoot in the mean Argon temperature along with a steep Argon temperature profile relative to Helium. While a clear overshoot is not visible in the corresponding MD profiles either, it is clearly visible that the mean Argon temperature exhibits a steeper profile than that of Helium. Interestingly, while well within the margin of error of the reported values, the opposite trend can be seen in the experimental values, in which Helium has a steeper mean temperature profile than that of Argon.

In all cases, the overall inflow and outflow temperature for MD was greater than that for the experiment. This was, in part, due to the assumption of a higher inflow temperature which was used for MD than that seen in the experimental temperature profiles. Also, due to the less than dilute nature of the gas within the MD simulation, a higher outflow temperature developed than was predicted.

3.2 DSMC Comparison of Helium-Argon and Helium-Xenon Gas Mixtures

In addition to the experiment, shock profiles generated by MD were compared to results generated by DSMC. These include Generalized Hard Sphere GHS-DSMC simulations by Hassan and Hash of shock structures composed of 11.5% Argon-88.5% Helium and 1.5% Xenon-98.5% Helium and a Hard Sphere HS-DSMC simulation by Bird for a shock structure composed of 50% Argon-50% Helium. The Mach number and inflow free stream temperatures for these cases are 1.58 and 162.5 K, 3.61 and 300 K, and 10 and 150 K, respectively. Normalized density profiles for 11.5%-Argon and 1.5%-

Xenon are shown in Figures 3.13 and 3.16, respectively, and normalized temperature profiles for 11.5%-Argon are shown in Figures 3.14 and 3.15. Agreement between all MD and GHS-DSMC profiles are extremely good with virtually overlapping profiles. The hard sphere approximation used by Bird for 50%-Argon does not agree as well with MD as GHS-DSMC does, as seen by the normalized velocity, temperature, and molar ratio profiles shown in Figures 3.17 through 3.19. This was expected, though, due to HS-DSMC's inability to model attractive-repulsive forces.[5] However, trends between Argon and Helium for velocity, temperature, and molar ratio agree very well with expected results.

For 11.5%-Argon, Hassan and Hash also compared their GHS-DSMC results to the experimental data of Harnett and Muntz used above. These experimental results are included in the comparison of MD and GHS-DSMC for 11.5%-Argon. The MD results used for this comparison are the same as those used above for 11.5%-Argon, but rescaled and normalized. Due to uncertainty by Hassan and Hash in the length scale used by Harnett and Muntz, they used an unspecified length scaling factor, *L,* that best fit the experimental data. Therefore, the MD results for 11.5%-Argon were also rescaled using a length scaling factor that provided a best fit with their GHS-DSMC results. This resulted in a length scaling factor, *L,* of 492 Å being applied to the MD profiles. Local densities and temperatures were normalized by:

$$\rho' = \frac{\rho - \rho_1}{\rho_2 - \rho_1} \tag{3.4}$$

and

$$T' = \frac{T - T_1}{T_2 - T_1} \tag{3.5}$$

where ρ and T are the local density and temperature, respectively, and the subscripts 1 and 2 indicate inflow and outflow conditions, respectively. Normalized profiles for density, parallel and perpendicular Argon temperatures, and parallel and perpendicular Helium temperatures for 11.5%-Argon are shown below:

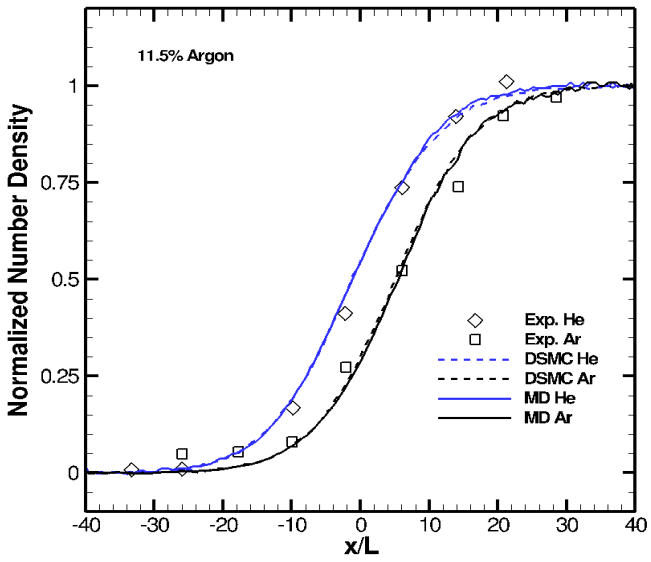

Figure 3.13: Normalized number density of Argon (square for experiment, dotted black line for GHS-DSMC, solid black line for MD) and Helium (diamond for experiment, dotted blue line for GHS-DSMC, solid blue line for MD) for 11.5%-Argon mixture.

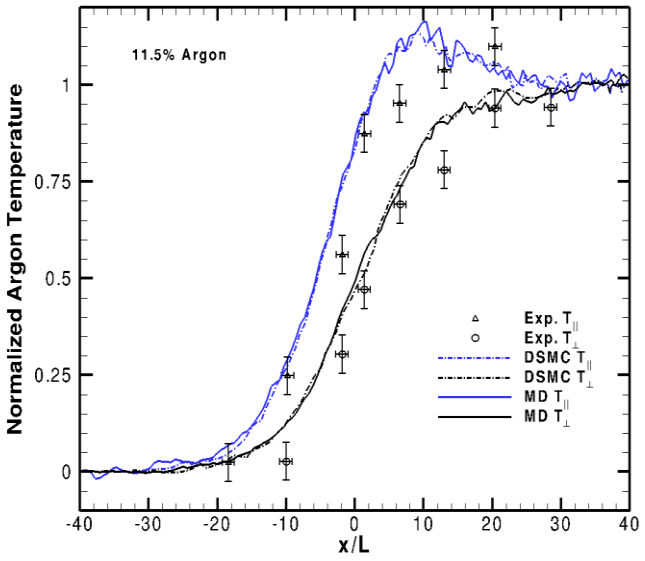

Figure 3.14: Normalized perpendicular (circles for experiment, dashed black line for GHS-DSMC, solid black line for MD) and parallel (triangle for experiment, dashed blue line for GHS-DSMC, solid blue line for MD) temperature profiles of Argon for 11.5%-Argon mixture.

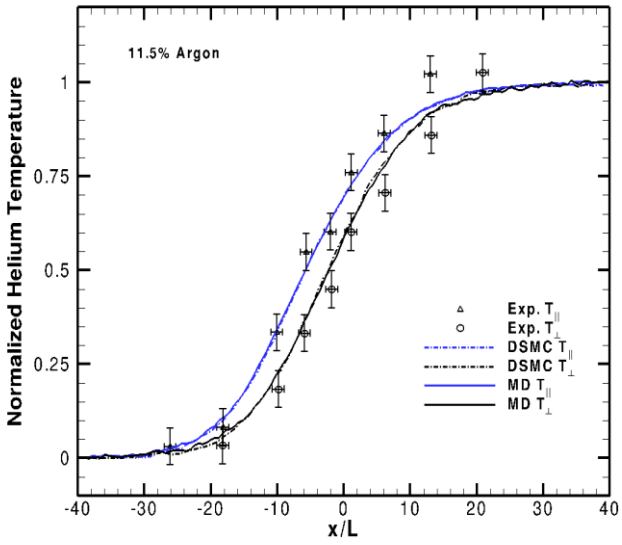

Figure 3.15: Normalized perpendicular (circles for experiment, dashed black line for GHS-DSMC, solid black line for MD) and parallel (triangle for experiment, dashed blue line for GHS-DSMC, solid blue line for MD) temperature profiles of Argon for 11.5%-Argon mixture.

Results between GHS-DSMC and MD are extremely good for all profiles. Interestingly, the parallel temperature overshoot for Argon seen in Figures 3.4 and 3.14 that Harnett and Muntz attributed to measurement error are clearly defined in both MD and GHS-DSMC profiles. Note that while Hassan and Hash site the paper by Harnett and Muntz used above, it is unclear where they found the number density profiles for Harnett and Muntz's experimental values.

For the 1.5%-Xenon mixture shock, an inflow density of $\rho_1 = 0.5\ \mathrm{kg/m^3}$ was chosen based on the same limitations as described for the 11.5%-Argon, 24.7%-Argon, and 44%-Argon MD cases above. However, because the inflow temperature and Mach numbers are much higher than the Argon-Helium cases above, the non-dilute effects of the gas are not noticeable. While a length scaling factor is not expressly defined by Hassan and Hash for this case, it is inferred that the length scale is normalized with the upstream mean free path, λ_1, which can be approximated by:[18]

$$\lambda_1 \cong \frac{16}{5}\sqrt{\frac{\gamma}{2\pi}}\frac{\mu(T_1)}{\rho_1 a_1} \tag{3.6}$$

where γ is the heat capacity ratio of a monatomic gas, ρ_1 and a_1 are the inflow density and speed of sound, respectively, and $\mu(T_1)$ is the upstream shear viscosity of the mixture derived from Appendix A given the inflow temperature T_1. This provides a length scaling factor, λ_1, of 833 Å. However, because the true derivation of λ_1 by Hassan and Hash is unclear, it was deemed reasonable to increase λ_1 to 840 Å to provide a better fit

to their data. The number density was normalized using Equation 3.4.

The normalized number density for 1.5%-Xenon comparing GHS-DSMC and MD is shown below:

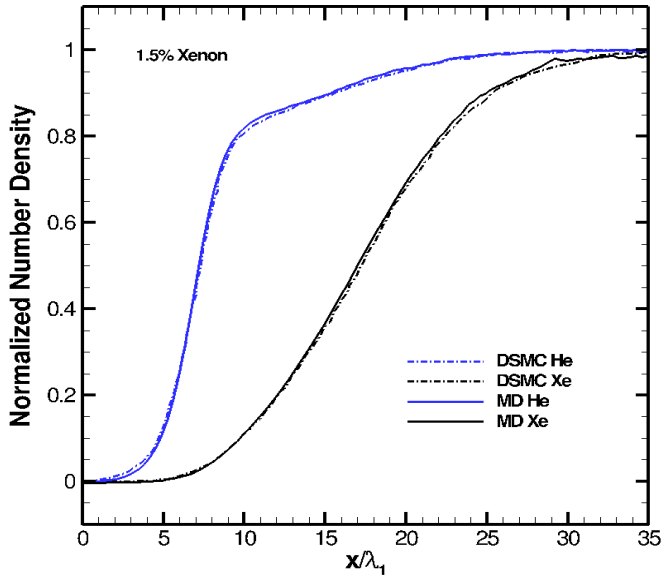

Figure 3.16: Normalized number density of Xenon (dotted black line for GHS-DSMC, solid black line for MD) and Helium (dotted blue line for GHS-DSMC, solid blue line for MD) for 1.5%-Xenon mixture.

Again, as with 11.5%-Argon, MD is in excellent agreement with GHS-DSMC even with a more rigid scaling factor.

For the 50%-Argon shock, an inflow density of $\rho_1 = 0.5\ \text{kg/m}^3$ was chosen based on the same limitations in the MD simulation box length described above. However, in this case, the inflow temperature $T_1 = 150$ K was not explicitly given by Bird and was instead chosen to provide a reasonable outflow temperature, which at Mach 10 was $T_2 = 4818$ K. Discrepancies between the set inflow and outflow temperatures and

densities with those developed by the shock within MD were noticeable. The inflow and outflow temperatures were 1.2% and 0.7% hotter, respectively, and the outflow density was 0.77% lower than expected. While this was due in part to the non-dilute nature of the gas, the simulation box may have additionally been too small to allow a smooth transition between inflow and outflow free stream conditions. In terms of mean free path λ_1, the box length for 50%-Argon was approximately $35\lambda_1$ compared to $40\lambda_1$ for the other Argon-Helium MD simulations. The length scale factor used by Bird is the hard sphere approximation of the inflow mean free path λ_0 for a binary gas mixture, given by:

$$\lambda_0 = \frac{1}{\pi\left(n_{1,1} + n_{1,2}\right)}\left[\frac{n_{1,1}}{\sqrt{2}n_{1,1}{\sigma_1}^2 + n_{1,2}\left\{\frac{(\sigma_1+\sigma_2)^2}{4}\right\}\sqrt{1+\frac{m_1}{m_2}}} + \frac{n_{1,2}}{\sqrt{2}n_{1,2}{\sigma_2}^2 + n_{1,1}\left\{\frac{(\sigma_1+\sigma_2)^2}{4}\right\}\sqrt{1+\frac{m_2}{m_1}}}\right] \tag{3.7}$$

where $n_{1,1}$ and $n_{1,2}$ are the inflow number densities, σ_1 and σ_2 are hard sphere diameters, and m_1 and m_2 are the particle masses, of each species respectively. Using the Van der Waals radius to approximate the hard sphere radius of Argon and Helium, $\sigma_{Ar} = 3.76$ Å and $\sigma_{He} = 2.8$ Å, respectively.[15] For the 50%-Argon case, the mean free path λ_0 was found to be 1455 Å. Bird normalized the velocity and temperature profiles by dividing the local velocity by the inflow free stream speed of sound a_1 and the local temperature by the inflow free stream temperature T_1, respectively. The molar ratio profile is simply

the local number density for Helium divided by the local number density for Argon. The velocity, temperature, and molar fraction profiles for 50%-Argon are shown below:

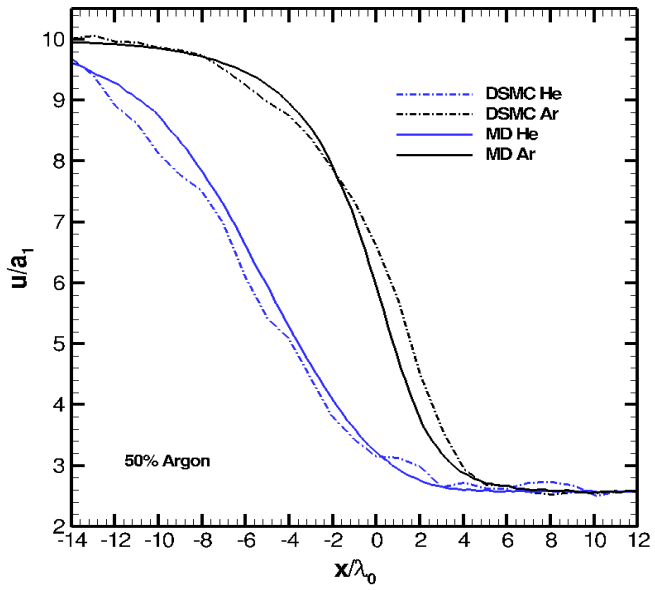

Figure 3.17: Normalized velocity of Argon (dotted black line for HS-DSMC, solid black line for MD) and Helium (dotted blue line for HS-DSMC, solid blue line for MD) for 50%-Argon mixture.

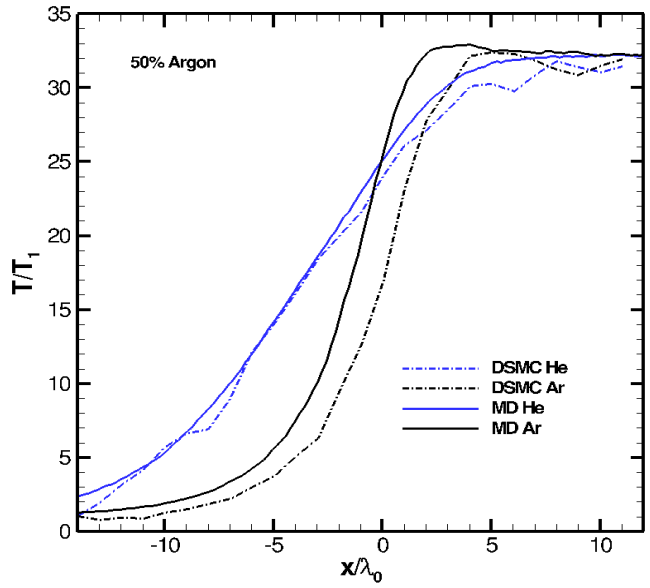

Figure 3.18: Normalized average temperature of Argon (dotted black line for HS-DSMC, solid black line for MD) and Helium (dotted blue line for HS-DSMC, solid blue line for MD) for 50%-Argon mixture.

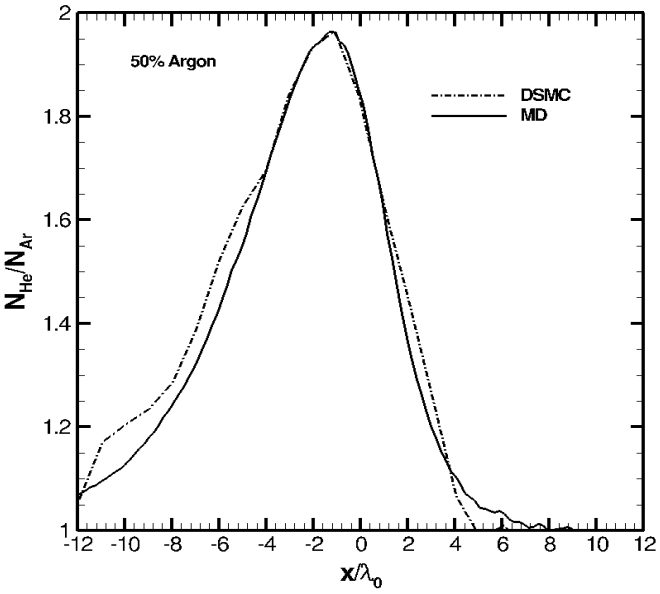

Figure 3.19: Molar fraction N_{He}/N_{Ar} (dotted line HS-DSMC, solid line MD) for 50%-Argon.

While good correlation between HS-DSMC and MD was never expected, profiles for normalized velocity and molar fraction are in good agreement with each other. An overshoot in the mean Argon temperature along with a steep Argon temperature profile is clearly visible in Figure 3.18. As discussed above in the experimental results of Harnett and Muntz, this trend was expected but not clearly visible in their results or MD due the low Mach number associated with their experiments. At the higher Mach number associated with 50%-Argon, this trend is clearly visible. The separation in concentrations of Argon and Helium shown in Figure 3.19 is understandable due to the early development of the Helium velocity profile relative to Argon as shown in Figure 3.17. This resulted in a lower velocity relative to Argon, leading to an increased Helium mole fraction at the center of the shock due to continuity.

It was demonstrated by Bird that the degree of species separation within the shock would increase with shock Mach number. This can be seen by comparing the normalized weighted Helium mole fraction, M'_{He}, from the 11.5%, 24.7%, 44%, and 50%-Argon cases shown in Figure 3.20, where M'_{He} is given by:

$$M'_{He} = \frac{M_{He}(x) - M_{He,1}}{M_{Ar,1}} \tag{3.8}$$

where $M_{He}(x)$ is the mole fraction of Helium and $M_{He,1}$ is the free stream mole fraction of Helium. The length scale factor, *L*, used for 50%-Argon was determined to be *L* = 842 Å using the same method as that for 11.5%, 24.7% and 44%-Argon in Section 3.1.

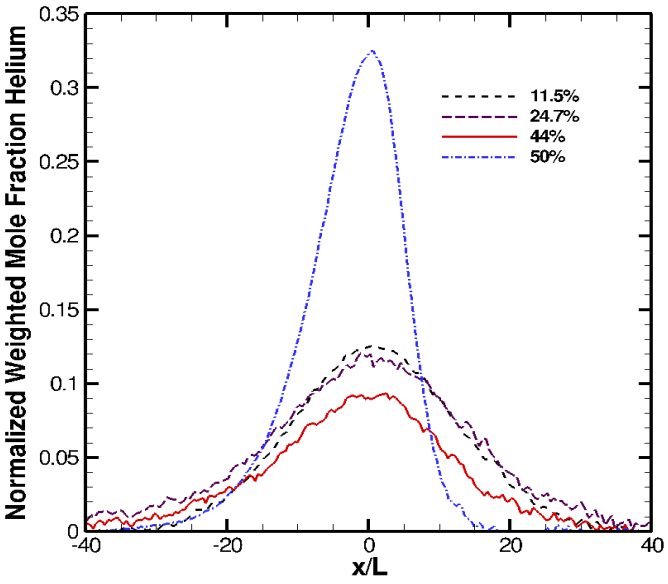

Figure 3.20: Normalized weighted mole fraction Helium for 11.5%-Argon (black) Mach 1.65, 24.7%-Argon (purple) Mach 1.58, 45%-Argon (red) Mach 1.65, and 50%-Argon (blue) Mach 10.

As can be seen from Figure 3.20, the relative separation of Helium from Argon for a Mach 10 flow is much greater than any of the other flows at lower Mach numbers. This agrees with Bird's findings showing a higher degree of separation at higher Mach numbers.

3.3 Experimental Comparison of Nitrogen Shock Structures

Experiments by Robben and Talbot[2] were measured using an electron beam fluorescence technique that included a shock structure composed of pure Nitrogen at Mach 7. Normalized profiles for density and rotational temperature are shown in Figure 3.21. A comparison between MD and experiment shows a slightly thicker profile for

both density and rotational temperature in MD, along with a slightly larger separation between density and rotational temperature profiles. The inflow temperature measured by Robben and Talbot, and used in MD, was 28.3K. An inflow density of 0.1 kg/m^3 was chosen for the MD simulations to minimize any non-dilute effects of the gas at such a low inflow temperature. A length scaling factor, *L*, of 228 Å was used to scale the MD profiles to Robben and Talbot's data. Although the length scaling factor, *L*, is defined in Equation 3.1, the value used here was arbitrarily chosen to provide the best results with Robben and Talbot's normalized density profile for Nitrogen. This was necessary due to the unknown shear viscosity at sonic conditions attributed to the Lennard-Jones parameters used to model the flow. The Lennard-Jones parameters for atomic Nitrogen were taken from Matsumoto[21], who used DSMC to simulate the experimental results of Robben and Talbot using the Dynamic Molecular Collision (DMC) model. Molecules within the MD simulation were modeled as rigid rotors with a fixed bond length of r_0; this was done to prevent the effects of vibrational energy present in a classical MD simulation that do not realistically exist at the temperatures considered here. Density and temperature profiles were normalized using Equations 3.4 and 3.5, respectively. The normalized density and rotational temperature profiles for Nitrogen at Mach 7 and T_1 = 28 K are shown below:

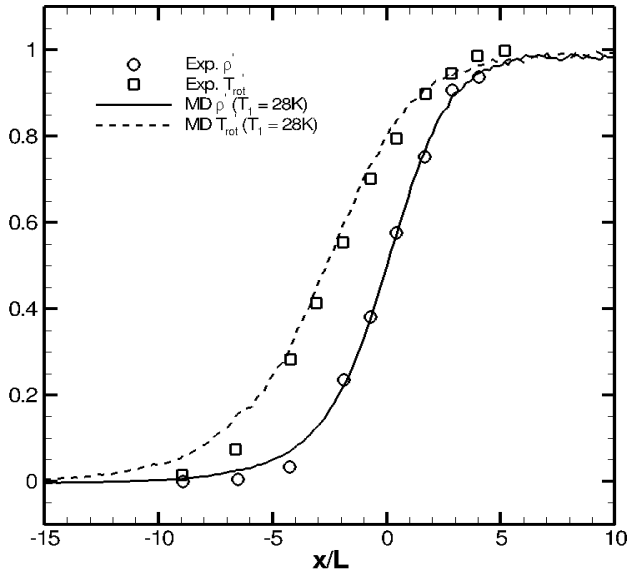

Figure 3.21: Normalized density (circle for experiment, solid line for MD) and rotational temperature (square for experiment, dashed line for MD) of Nitrogen at Mach 7 and T_1 = 28 K.

With a length scaling factor defined by the normalized density, the separation between density and rotational temperature profiles is slightly larger in MD than seen by experiment. MD also shows a slightly thicker profile for both density and rotational temperature, where both profiles begin to develop before experiment.

In addition to the MD simulation of Nitrogen with an inflow Mach number of 7 and an inflow temperature of 28 K, a simulation with an inflow temperature of 300 K was considered. Normalized density and rotational temperature profiles T_1 = 300 K and T_1 = 28 K are shown in Figure 3.22 along with Robben and Talbot's experimental results. Normalized density profiles for MD at T_1 = 28 K and T_1 = 300 K are nearly identical. Normalized rotational temperature profiles show similar thickness and structure between

T_1 = 300 K and T_1 = 28 K; however, the separation between the normalized density and rotational temperature is less at T_1 = 300 K. A length scaling factor, L, of 516 Å was used to scale the MD profiles at T_1 = 300 K. As before, this factor was chosen to provide the best fit with the normalized density profile of Robben and Talbot. The normalized density and rotational temperature profiles for Nitrogen at Mach 7 are shown below:

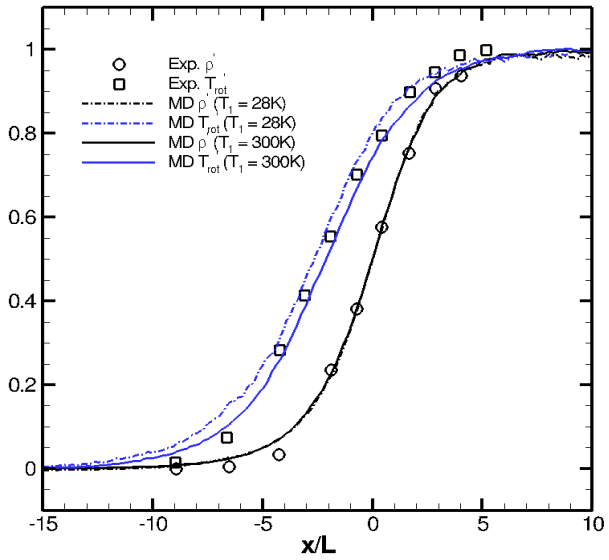

Figure 3.22: Normalized density (circle for experiment, black lines for MD) and rotational temperature (square for experiment, blue lines for MD) of Nitrogen at Mach 7 and T_1 = 28 K (dashed lines for MD) and T_1 = 300 K (solid lines for MD).

While the normalized density profiles and overall shock thickness are very similar between MD simulations at T_1 = 28 K and T_1 = 300 K, separation between the two profiles is noticeably less at T_1 = 300 K. Compared to experiment, separation between normalized density and rotational temperature profiles for T_1 = 28 K is greater, while at T_1 = 300 K separation is less, with neither providing better agreement with experiment.

4 Conclusion

In this work, the structures of normal shock waves in dilute Nitrogen and mixtures of Helium-Argon and Helium-Xenon have been simulated using large-scale molecular dynamics. These results were compared to a series of experimental data and DSMC simulations to provide a validation of the MD technique.

For MD simulations of normal shock waves comprised of 11.5% Argon-88.5% Helium, 24.7% Argon-75.3% Helium, and 44% Argon-56% Helium, agreement with experiment is promising. Velocity profiles compare favorably with experiment, while mean temperature profiles and parallel and perpendicular Helium temperature profiles show expected separation trends; however, an exact comparison was difficult due to non-dilute effects within the MD simulation. The Argon parallel temperature profiles at 11.5%-Argon for MD are well-matched with experiment and GHS-DSMC despite the assertion of Harnett and Muntz that any trend in that data was due to measurement uncertainty.

Comparisons between GHS-DSMC and MD for 11.5%-Argon and 1.5%-Argon showed near perfect agreement with each other in all compared quantities. As expected, HS-DSMC for 50%-Argon showed poor agreement with MD due to the inability for a hard sphere model to simulate attractive and repulsive forces. However, trends in temperature and molar fraction not seen in the lower Mach number cases were clearly visible at Mach 10 and agreed with expected results.

Nitrogen profiles for rotational temperature and density were in good agreement with experiment at Mach 7 and T_1 = 28.3 K, with a slightly larger separation between

density and rotational temperature profiles and an overall, slightly thicker shock shown in MD. An additional simulation with an inflow temperature T_1 = 300 K showed a decrease in separation between normalized density and rotational temperature profiles. Both simulations assumed a rigid rotor molecular model to insure the vibrational energy effect normally present at the higher temperatures did not contribute to variations between the two profiles.

Overall, MD performed as expected and provided good to excellent agreement between MD, DSMC, and experimental data within a highly non-equilibrium system using only intermolecular potentials. Therefore, MD may represent a valuable tool for validating more computationally efficient methods for solving complex flows for which reliable experimental data does not exist.

Bibliography

[1] L. N. Harnett and E. P. Muntz, "Experimental investigation of normal shock wave velocity distribution functions in mixtures of Argon and Helium," Phys. Fluids 15, 565 (1972)

[2] Robben, F. and Talbot, L., "Experimental Study of the Rotational Distribution Function of Nitrogen in a Shock Wave", Phys. Fluids, Vol.9 (1964), pp.653-662

[3] Alsmeyer, H., "Density profiles in argon and nitrogen shock waves measured by the absorption of an electron beam," J. Fluid Mech., Vol. 74, No. 2, Jul 1976, pp. 497-513

[4] G. A. Bird, "The structure of normal shock waves in a binary gas mixture," J. Fluid Mech., Vol. 31, part 4 (1968), pp. 657-668

[5] H. A. Hassan and D. B Hash, "A generalized hard-sphere model for Monte Carlo simulation," Phys. Fluids A 5 (3), 1993, pp. 738-744

[6] H. Matsumoto, "Transport Coefficients of Inelastic Collision Model in the Direct Simulation Monte Carlo Method," JSME, Series B, Vol. 49, No. 3, 2006, pp. 780-786

[7] T. E. Schwartzentruber and P. Valentini, "Molecular Dynamics Simulations of Normal Shocks in Dilute Gases," 41st AIAA Thermophysics Conference, 22-25 June 2009, San Antonio, Texas

[8] S. Plimpton, "Fast Parallel Algorithms for Short-Range Molecular Dynamics," J Comp Phys, 117, 1-19 (1995), The LAMMPS website <http://lammps.sandia.gov>

[9] P. Hill and C. Peterson, "Mechanics and Thermodynamics of Propulsion," Second Edition, Addison-Wesley Publish Company, 1992, pp. 83-84

[10] Weisstein, Eric W. "Sphere Point Picking." From MathWorld--A Wolfram Web Resource. http://mathworld.wolfram.com/SpherePointPicking.html

[11] A. M. Kuethe and C. Chow, "Foundations of Aerodynamics, Bases of Aerodynamic Design," Fifth Edition, John Wiley & Sons, Inc., 1998, pp. 248

[12] D. A. McQuarrie, "Statistical Mechanics," University Science Books, 2000

[13] W. G. Vincenti and C. H. Kruger, "Introduction to Physical Gas Dynamics," Krieger Publishing Company, 1965

[14] Weisstein, Eric W. "Normal Distribution." From MathWorld--A Wolfram Web Resource. http://mathworld.wolfram.com/NormalDistribution.html

[15] David R. Lide, ed., "CRC Handbook of Chemistry and Physics", 89th Edition (Internet Version 2009), CRC Press/Taylor and Francis, Boca Raton, FL

[16] D. A. McQuarrie and J. D. Simon, "Physical Chemistry, A Molecular Approach," University Science Books, 1997

[17] F. Robben and L. Talbot, "Measurment of Shock Wave Thickness by the Electron Beam Fluorescence Method," Phys. Fluids, Vol. 9, Num. 4, April 1966, pp. 633-643

[18] P. Valentini and T. E. Schwartzentruber, "Large-scale molecular dynamics simulations of normal shock waves in dilute argon," Phys. Fluids 21, 066101 (2009)

[19] J. O. Hirschfelder, C. F. Curtiss, and R. B. Bird, "Molecular Theory of Gases and Liquids," John Wiley & Sons, 1954

[20] Chapman & Cowling, "The Mathematical Theory of Non-Uniform Gases", Third Edition, p.241 (Table 19)

[21] T. Tokumasu and Y. Matsumoto, "Dynamic molecular collision (DMC) model for rarefied gas flow simulations by the DSMC method," Phys. of Fluids, Vol. 11, Num. 7, July 1999, pp. 1907-1919

Appendix A: Viscosity Calculation

The viscosity of a multicomponent mixture is approximated using kinetic theory. To the 1st-approximation, the viscosity of a *v*-component mixture is given by:

$$[\mu_{mix}]_1 = -\frac{\begin{vmatrix} H_{11} & H_{12} & H_{13} & \cdots & H_{1v} & x_1 \\ H_{12} & H_{22} & H_{23} & \cdots & H_{2v} & x_2 \\ H_{13} & H_{23} & H_{33} & \cdots & H_{3v} & x_3 \\ \vdots & \vdots & \vdots & \ddots & \vdots & \vdots \\ H_{1v} & H_{2v} & H_{3v} & \cdots & H_{vv} & x_v \\ x_1 & x_2 & x_3 & \cdots & x_v & 0 \end{vmatrix}}{\begin{vmatrix} H_{11} & H_{12} & H_{13} & \cdots & H_{1v} \\ H_{12} & H_{22} & H_{23} & \cdots & H_{2v} \\ H_{13} & H_{23} & H_{33} & \cdots & H_{3v} \\ \vdots & \vdots & \vdots & \ddots & \vdots \\ H_{1v} & H_{2v} & H_{3v} & \cdots & H_{vv} \end{vmatrix}} \tag{A.1}$$

Where x_v equals the mole fraction of the *i*th component. The factors H_{ii} and H_{ij} are defined as:

$$H_{ii} = \frac{{x_i}^2}{[\mu_{ii}]_1} + \sum_{\substack{k=1 \\ k\neq i}}^{v} \frac{2x_i x_k}{[\mu_{ik}]_1} \frac{M_i M_k}{(M_i + M_k)^2} \left[\frac{5}{3\mathrm{A}_{ik}{}^{\star}} + \frac{M_k}{M_i}\right] \tag{A.2}$$

$$H_{ij} = -\frac{2x_i x_j}{[\mu_{ij}]_1} \frac{M_i M_j}{(M_i + M_j)^2} \left[\frac{5}{3\mathrm{A}_{ij}{}^{\star}} - 1\right] \quad i \neq j \tag{A.3}$$

where M_i is the molecular weight of the *i*th component and $[\mu_{ij}]_1$ is the 1st-approximation of the viscosity of a binary mixture.

The viscosity of a binary mixture is given by:

$$\left[\mu_{ij}\right]_1 \times 10^7 = 266.93 \frac{\sqrt{2M_iM_jT/\left(M_i + M_j\right)}}{{\sigma_{ij}}^2 \Omega_{\mathrm{ij}}^{(2,2)\star}({T_{12}}^*)} \tag{A.4}$$

where σ_{ij} is the collision diameter in Å as defined by the Lenard-Jones potential between components *i* and *j*.

The value A^* is defined as $\Omega^{(2,2)\star}/\Omega^{(1,1)\star}$ where $\Omega^{(l,s)\star}$ indicates the integral associated with the interaction between species *i* and *j*, and has the physical significance that indicates the deviation of any particular molecular model from the idealized rigid-sphere model. Quantities A^* and $\Omega^{(2,2)\star}$ for the Lennard-Jones (6-12) potential can be found in Reference [19] for a range of reduced temperatures T^* defined by:

$${T_{ij}}^* = \frac{kT}{\epsilon_{ij}} \tag{A.5}$$

where ϵ_{ij}/k is the Lennard-Jones potential in Kelvin and T is the temperature in Kelvin. A validation of this method is shown below with a comparison of calculated viscosity to experimental data[20] for Helium-Argon mixtures at 293.15 K

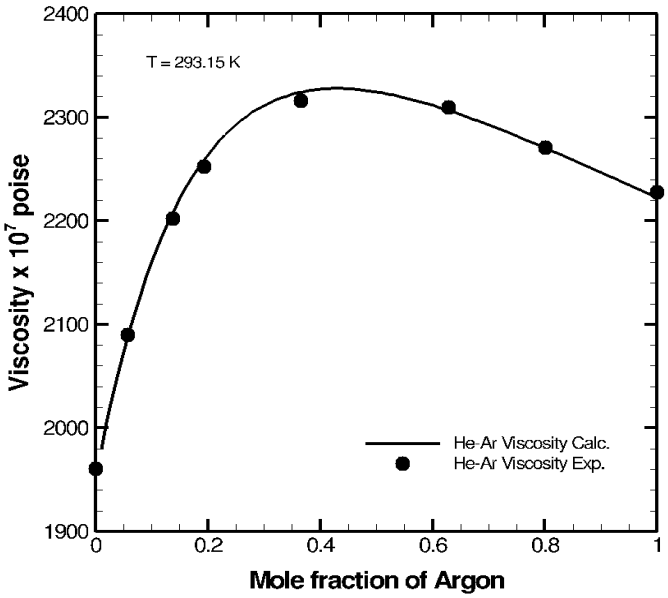

Figure A.1: Calculated viscosity (solid line) and experimental viscosity (circles) for Helium-Argon at 293.15 K.